Zoological Journal of the Linnean Society, 2023, XX, 1–30
https://doi.org/10.1093/zoolinnean/zlad121
Advance access publication 28 September 2023
Original Article

OXFORD

Original Article

Phylogenetic history of golden moles and tenrecs (Mammalia: Afrotheria)

Gary N. Bronner,[1] Samantha Mynhardt[2,*], Nigel C. Bennett,[3] Lientjie Cohen,[4] Nick Crumpton,[5] Michael Hofreiter,[6] Patrick Arnold,[6] Robert J. Asher[7,*]

[1]Institute for Communities and Wildlife in Africa, Department of Biological Sciences, University of Cape Town, Cape Town, South Africa
[2]Department of Botany and Zoology, Stellenbosch University, Stellenbosch, South Africa
[3]Department of Zoology and Entomology, University of Pretoria, Pretoria, South Africa
[4]Mpumalanga Tourism and Parks Agency, Lydenburg, South Africa
[5]The Natural History Museum, London, United Kingdom
[6]Institute for Biochemistry and Biology, University of Potsdam, Potsdam, Germany
[7]Department of Zoology, University of Cambridge, Cambridge, United Kingdom

[*]Corresponding authors. Department of Botany and Zoology, Stellenbosch University, Private Bag X1 Matieland, 7602, Stellenbosch, South Africa. E-mail: smynhardt@sun.ac.za; Department of Zoology, University of Cambridge, Downing St., CB2 3EJ Cambridge, United Kingdom. E-mail: r.asher@zoo.cam.ac.uk

ABSTRACT

We conducted a phylogenetic analysis of genetic and anatomical data focusing on golden moles (Chrysochloridae) and tenrecs (Tenrecidae). Our results support the now well-resolved topology for extant tenrecids, in addition to the paraphyly of 'Chrysochlorinae' and the genera *Chrysochloris* and *Chlorotalpa* as traditionally used. *Carpitalpa arendsi* is the sister taxon to *Neamblysomus*; together, they compose the sister clade of *Amblysomus*. Unexpectedly, *Calcochloris obtusirostris* is the sister taxon of *Chrysospalax*. The oldest divergence within crown Chrysochloridae is likely to be the node separating *Eremitalpa–Huetia* or *Eremitalpa* alone from the remaining species. A *Chrysochloris–Cryptochloris* root appears most frequently under equally weighted parsimony or with few or no sampled tenrecids, suggesting that it is artefactual. The tropical genus *Huetia* is among the most widely distributed and anatomically polymorphic in our sample. *Eremitalpa* and *Huetia* have a relatively unspecialized hyoid apparatus and short angular process of the dentary. These elements in *Huetia* show a particular resemblance to those of the Namibian fossil *Namachloris*, which we reconstruct as a stem chrysochlorid. Crown chrysochlorids are geologically younger than crown tenrecids and probably diversified in the Miocene around the same time as the tenrecid genus *Microgale*. Fossils of both groups from Eocliff in Namibia are probably late Eocene to early Miocene in age.

Keywords: adaptive convergence; Africa; character evolution; computed tomography; hyoid apparatus; Madagascar; osteology; phylogeny; skull anatomy

INTRODUCTION

Extant golden moles (Chrysochloridae Gray, 1825) comprise approximately 21 currently known species of small, subterranean mammals from sub-Saharan Africa. Most are known from South Africa; together, they comprise the sister group of tenrecs (Tenrecidae Gray, 1821) and are collectively part of Afrotheria (Stanhope *et al.* 1998, Asher and Seiffert 2010). About 30 tenrecid species are known from Madagascar and another three from equatorial Africa. The phylogeny of tenrecs has been reasonably stable for more than a decade, including the consensus view that the ecologically diverse, extant species on Madagascar form a monophyletic clade to the exclusion of the three extant, mainland African species (Olson and Goodman 2003, Asher and Hofreiter 2006, Poux *et al.* 2008, Everson *et al.* 2016). Although the absence of molecular data from fossil tenrecids limits a comparably high level of confidence, one or more fossil tenrecids from mainland Africa might nest within the Malagasy radiation (Asher and Hofreiter 2006).

The phylogenetic history of chrysochlorids is not as well known as that of tenrecids. Chrysochlorids exhibit many distinctive features (Hickman 1990, Skinner and Smithers 1990, MacPhee and Novacek 1993; Bronner and Bennett 2005), a

Received 8 March 2023; revised 21 July 2023; accepted 10 August 2023

few of which are characteristic of fossorial mammals in general. In the postcranial skeleton, some of their more unusual traits include a mediolaterally compressed humeral head, a deltoid trough, a greatly enlarged medial epicondyle of the humerus and a correspondingly large and curved olecranon process of the ulna, a radial flexor canal and ossified flexor tendon composing a third long bone of the forearm (Fig. 1; Puttick and Jarvis 1977), laterally and posteriorly projecting processes of the scapular spine, a comma-shaped first rib, a keeled and dorsally concave sternum (Fig. 2), a parallel ilium and pubis (Fig. 3), a ball-and-socket joint between the calcaneus and fibula, ventral tarsal sesamoids, and a laterally extensive astragalo-navicular joint (Fig. 4).

In the cranial skeleton, chrysochlorids usually exhibit a sinus connecting left and right auditory bullae, trabeculated in some species (Fig. 5; see Forster-Cooper 1928, Mason *et al.* 2017). The hyoid apparatus is particularly derived (Fig. 6), with most species showing a sharply angled and bulbous stylohyoid that articulates with the dentary (Bronner *et al.* 1990, Bronner 1991). Extant species show lateral extensions of the premaxilla (Fig. 7), are dentally zalambdodont, and lack upper molar metacones, with reduced (and sometimes absent) lower molar talonids (Fig. 8; Butler 1937, Asher and Sánchez-Villagra 2005, Asher 2019). Chrysochlorids show a tightly coiled cochlea with three or more turns (Crumpton *et al.* 2015), and some species exhibit enormous mallei and elongated incudes (Fig. 9; Forster-Cooper 1928, Simonetta 1968, von Mayer *et al.* 1995, Mason 2003, 2004, Mason *et al.* 2017).

The brain is hypercholinergic in the only two chrysochlorids studied to date (*Amblysomus hottentotus* Smith, 1829 and *Chrysochloris asiatica* Linnaeus 1758; Bhagwandin *et al.* 2020),

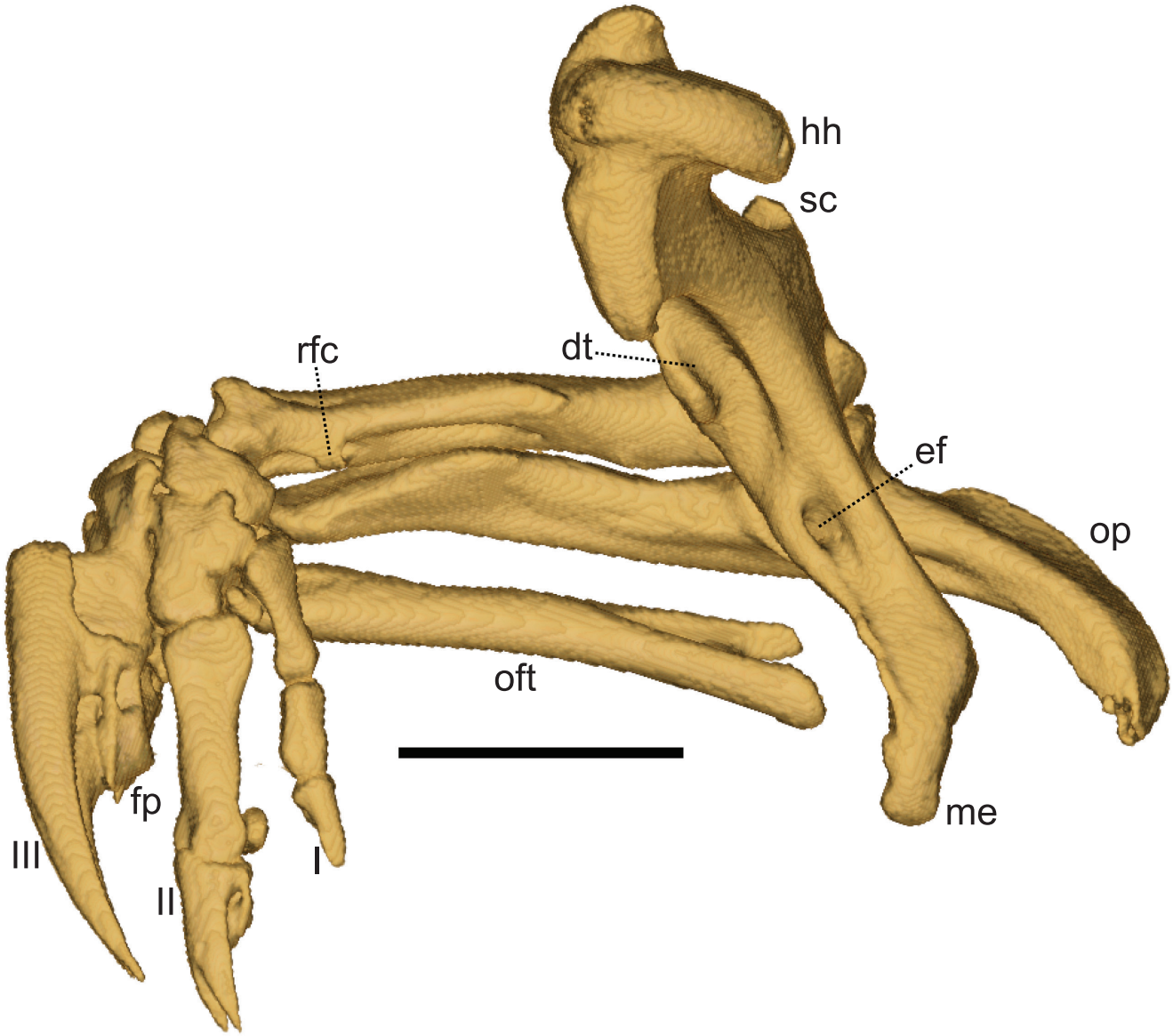

Figure 1. Right forelimb and hand skeleton of *Amblysomus corriae* in dorsal view (ZM 42553). Roman numerals indicate digital rays. Abbreviations: dt, deltoid trough; ef, entepicondylar foramen; fp, flexor process; hh, humeral head; me, medial epicondyle; oft, ossified flexor tendon; op, olecranon process; rfc, radius flexor canal; sc, supinator crest. Scale bar: 5 mm.

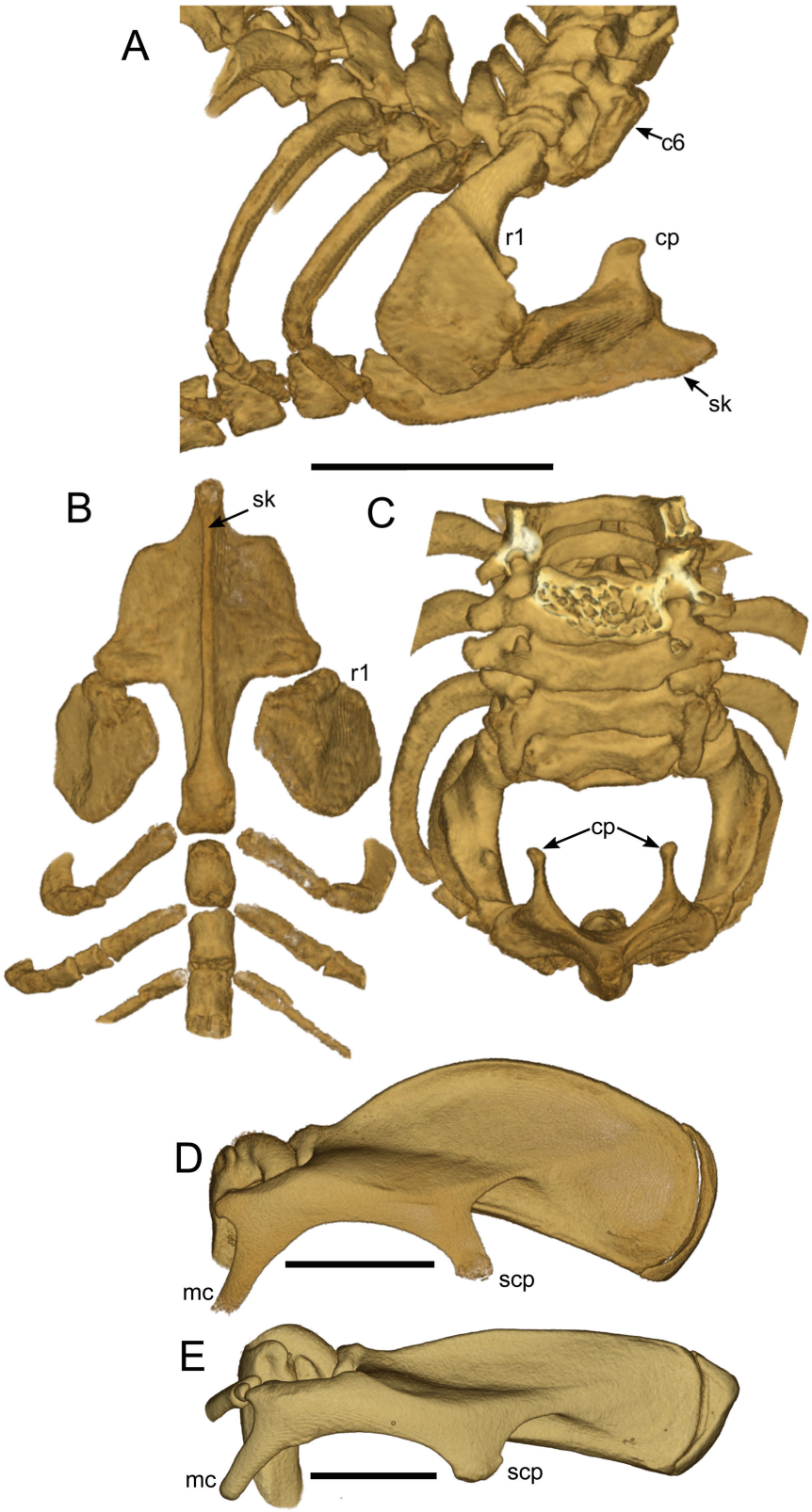

Figure 2. Sternum and proximal ribs of *Cryptochloris wintoni* (NRM-MA 641436) in lateral (A), ventral (B) and anterior (C) views. Dorsal views of scapulae of *Eremitalpa granti* (D; NRM-MA 641289) and *Chrysochloris asiatica* (E; MVZ 183379). Abbreviations: c6, sixth cervical vertebra; cp, clavicular process of sternum; mc, metacromion; r1, first rib; scp, scapular spine caudal process; sk, sternal keel. Scale bars (one for A–C): 5 mm.

and cholinergic nuclei involved in eye movement are reduced or absent. This is consistent with the vestigial eyes of golden moles, one of many convergent traits shown by small subterranean mammals (Partha *et al.* 2017). Given that the two species studied thus far represent disparate chrysochlorid branches (see Results), this could be another distinctive trait for some or all of the clade.

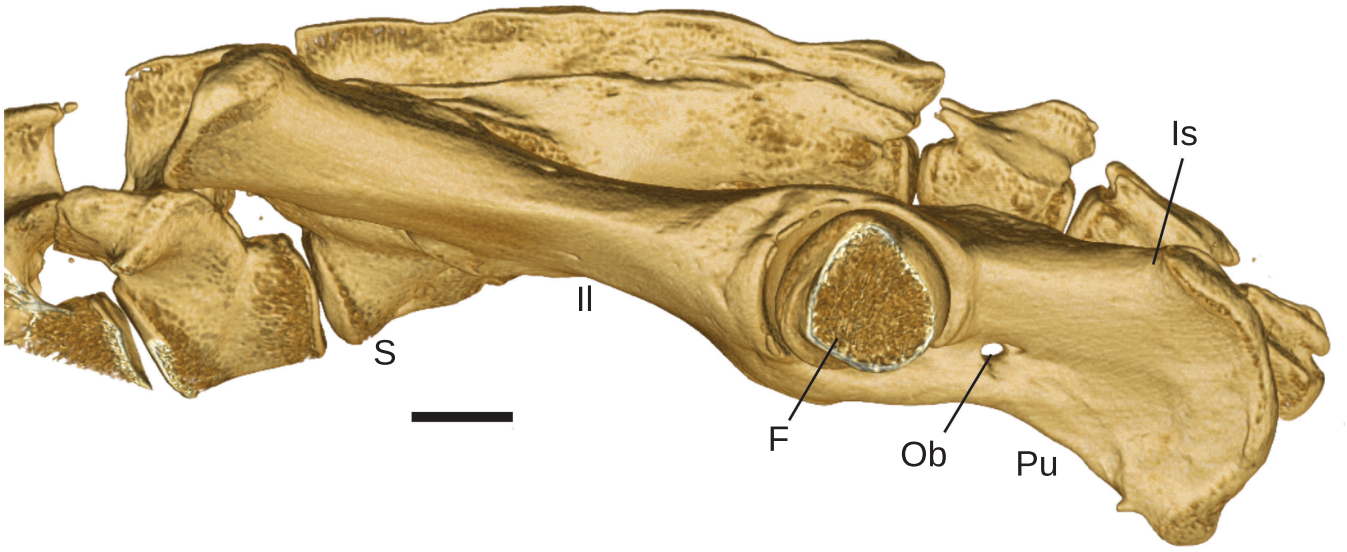

Figure 3. Pelvis in left lateral view of *Chrysospalax trevelyani* (UMZC E5470D). Abbreviations: F, femoral head; Il, ilium; Is, Ischium; Ob, obturator foramen; Pu, pubis; S, sacrum. Scale bar: 5 mm.

Chrysochlorids have relatively undifferentiated gastrointestinal tracts, consistent with their primarily insectivorous diet (Pinheiro *et al.* 2018), as in many other insect-eating and carnivorous mammals. Data for the more ecologically diverse tenrecs are scarce, but they too have simplified gastrointestinal tracts lacking a caecum, unlike macroscelidid afrotherians, which retain a caecum (Langer 2017) corresponding to their more omnivorous diet.

Karyotypically, golden moles are conserved, with most species having a diploid chromosome number of $2n = 30$. The exceptions are two cryptic lineages within the genus *Amblysomus* Pomel, 1848, which show $2n = 34$ (*Amblysomus septentrionalis* Roberts 1913) and $2n = 36$ (*Amblysomus robustus* Bronner, 2000; see Roberts 1951, Bronner 1995b). *Eremitalpa* Roberts, 1924 is another karyotypically distinctive chrysochlorid, with $2n = 26$ (Gilbert 2006, Gilbert *et al.* 2006, 2008). Collectively, these results suggest that chrysochlorids have more slowly or recently evolving chromosomes than most other high-level placental mammal clades.

Older classifications (e.g., Broom 1948a, Lundholm 1954, Simonetta 1968, Petter 1981) grouped taxa based largely on the morphology of their ear ossicles, placing species together with relatively small (e.g., *Amblysomus*, *Calcochloris* Mivart 1867; Fig. 9A), large and spherical (*Eremitalpa*, *Chrysospalax* Gill, 1883; Fig. 9C) or large and elongated (e.g., *Chrysochloris*, *Cryptochloris* Shortridge & Carter, 1938; Fig. 9D) mallei. Based on chromosomal and morphological data, Bronner (1995a: fig. 9.11) figured a root for Chrysochloridae among taxa with a large and elongated malleus by placing *Chrysochloris asiatica* as the sister taxon to all other chrysochlorids in his sample. Four recent phylogenetic analyses that sampled at least some genetic data from most chrysochlorid species (Asher *et al.* 2010, Faurby and Svenning 2015, Puttick and Thomas 2015, Upham *et al.* 2019) also contrasted with an ossicle-based phylogeny, with clades having a large malleus again appearing as one or more sister taxa to an *Amblysomus–Neamblysomus* Roberts, 1924–*Carpitalpa* Lundholm, 1954 group. Neither Asher *et al.* (2010) nor Puttick and Thomas (2015) nor Faurby and Svenning (2015) resolved the chrysochlorid root node, but Upham *et al.* (2019) depicted an *Eremitalpa–Huetia* Forcart, 1942 clade as the sister taxon to the remaining extant chrysochlorids. However, as indicated in their figure 1 caption, Upham *et al.* (2019) did not sample *Huetia* in their DNA alignment.

Among the many interesting questions regarding the acquisition of this unique suite of characters is the evolution of their auditory morphology. Phylogenetic hypotheses published since the 1990s (e.g., Bronner 1995a, b, Asher *et al.* 2010, Faurby and Svenning 2015, Puttick and Thomas 2015, Upham *et al.* 2019) have tended to place most taxa with generalized ossicular anatomy (*Amblysomus*, *Neamblysomus* and *Calcochloris obtusirostris* Peters 1851) in nested positions, far from the root taxon. As previously noted, candidates for the first divergent branch within Chrysochloridae include *Eremitalpa–Huetia* (Upham *et al.* 2019), *Chrysochloris* and *Chrysospalax* (Bronner 1995a), *Chrysochloris–Cryptochloris–Eremitalpa* (Faurby and Svenning 2015) and *Eremitalpa* (Asher *et al.* 2010: fig. 3). Most of these taxa possess some of the most derived auditory ossicles known among mammals.

Huetia leucorhinus Huet, 1885 is the exception. The species epithet has previously been written as '*leucorhina*' to match the perceived feminine gender of its Latinized generic names (Forcart 1942). Many first declension Latin nouns (ending in 'a') are feminine, but others are not. To maintain consistency with Bronner and Jenkins (2005) and Asher *et al.* (2010), we keep the spelling *Hu. leucorhinus*. This central- and west-African species was first placed in the genus *Chrysochloris* by Huet (1885) and has previously been assigned to the genera *Amblysomus* by Simonetta (1968), *Chlorotalpa* Roberts, 1924 by Meester (1974) and *Calcochloris* by Bronner (1995a, b), but was reassigned to *Huetia* at full generic rank by Asher *et al.* (2010). Some individuals of *Huetia* exhibit relatively small auditory ossicles (Bronner 1995a: 224; Mason *et al.* 2017: fig. 7d). In others, the mallear head is more dorsally expanded (Fig. 9B; see also Mason *et al.* 2017: fig. 7e).

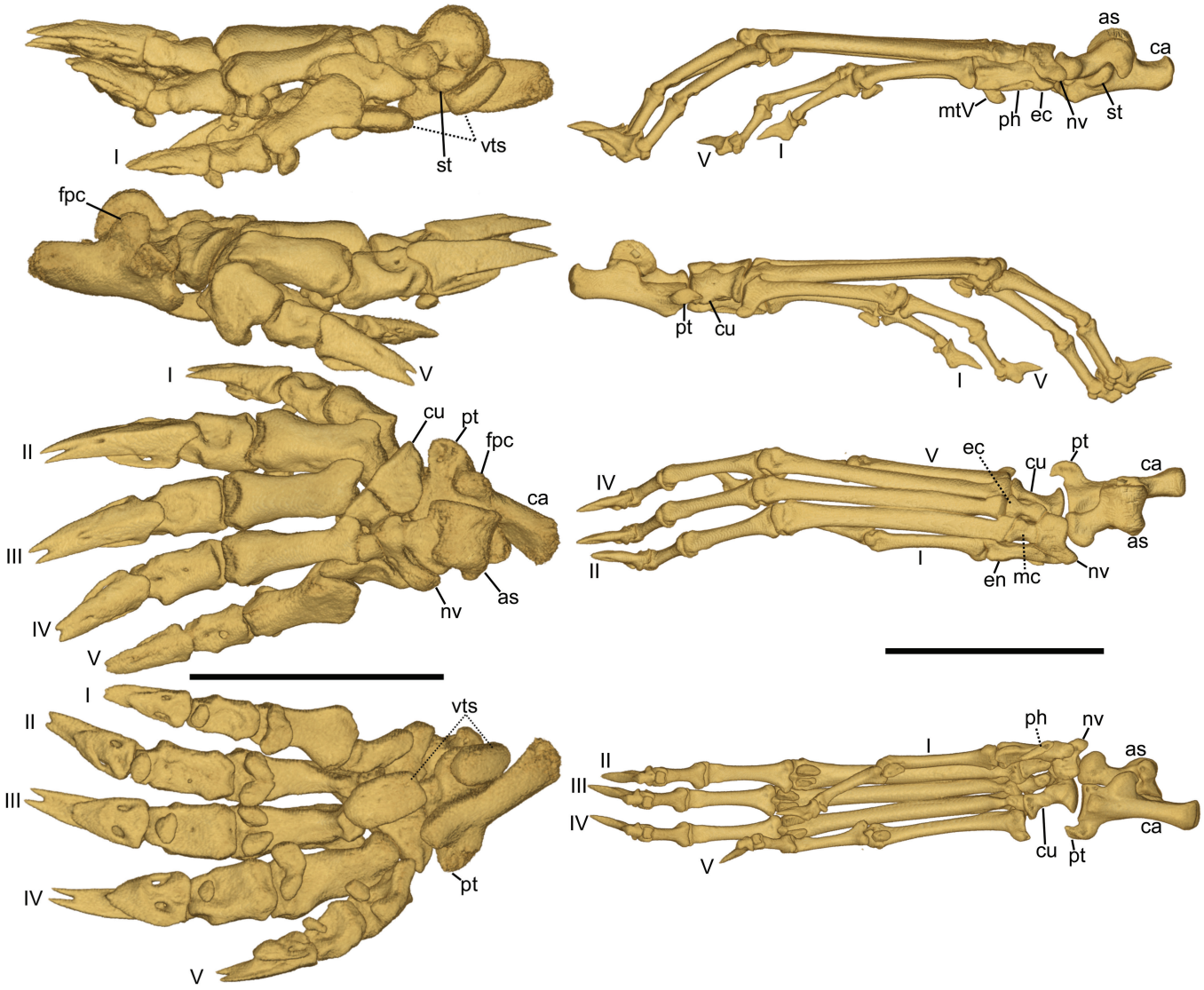

Figure 4. Right foot skeletons of *Cryptochloris wintoni* (left, NRM-MA 641436) and *Microgale cowani* (right, UMZC E5459A) in (from top to bottom) medial, lateral, dorsal and ventral views. Abbreviations: as, astragalus; ca, calcaneum; cu, cuboid; ec, ectocuneiform; en, entocuneiform; fpc, fibular process of calcaneum; mc, mesocuneiform; mtV, metatarsal V; nv, navicular; ph, prehallux; pt, peroneal tubercle; st, sustentacular tali of calcaneus; vts, ventral tarsal sesamoids. Roman numerals I, II, III, IV and V correspond to digits. Scale bars: 5 mm.

Chrysochlorid taxonomy

Simonetta's (1968: fig. 2) observation of specimens of *Hu. leucorhinus* with a relatively small malleus led him to assign that species to the genus *Amblysomus*. Likewise, he placed *Eremitalpa* and *Chrysospalax* together based on their large, spherical mallear heads (Fig. 9C), and recognized a group containing *Chrysochloris asiatica*, '*Chrysochloris*' *stuhlmanni* Matschie, 1894 and *Cryptochloris* based on their elongated mallear heads (Fig. 9D) and variably conspicuous temporal bullae (an external protuberance of the epitympanic recess, containing the incudo-mallear joint). Based on their typical possession of enlarged mallei, three molars and small talonids, he also added *Chlorotalpa sclateri* Broom, 1907, *Chlorotalpa duthieae* Broom, 1907 and *Carpitalpa arendsi* Lundholm, 1954 to this group.

Petter (1981) also used a classification that largely reflected middle ear anatomy, grouping taxa he considered to have small mallei in *Amblysomus*, those with spherical mallei in *Eremitalpa*–*Chrysospalax* and those with elongated mallei in *Chrysochloris*–*Cryptochloris*. Bronner (1995a: table 9.14) and Bronner and Jenkins (2005) incorporated a wider range of morphological and chromosomal data into their chrysochlorid classification. By placing *leucorhinus* as a species of *Calcochloris* within the Amblysominae, along with *Amblysomus*, *Neamblysomus* and *Calcochloris obtusirostris*, Bronner (1995a) and Bronner and Jenkins (2005) followed previous authors in implying consistency of mallear morphology with evolutionary history. Their other major group was the 'Chrysochlorinae', encompassing species with spherical (*Eremitalpa* and *Chrysospalax*), elongated (*Chrysochloris* and *Cryptochloris*) or slightly enlarged (*Chlorotalpa* and *Carpitalpa*) mallei.

Quantitative evaluations of morphological and chromosomal features (Bronner 1995a, b) and recent phylogenetic analyses (Asher *et al.* 2010, Faurby and Svenning 2015, Puttick and Thomas 2015, Upham *et al.* 2019) have suggested that

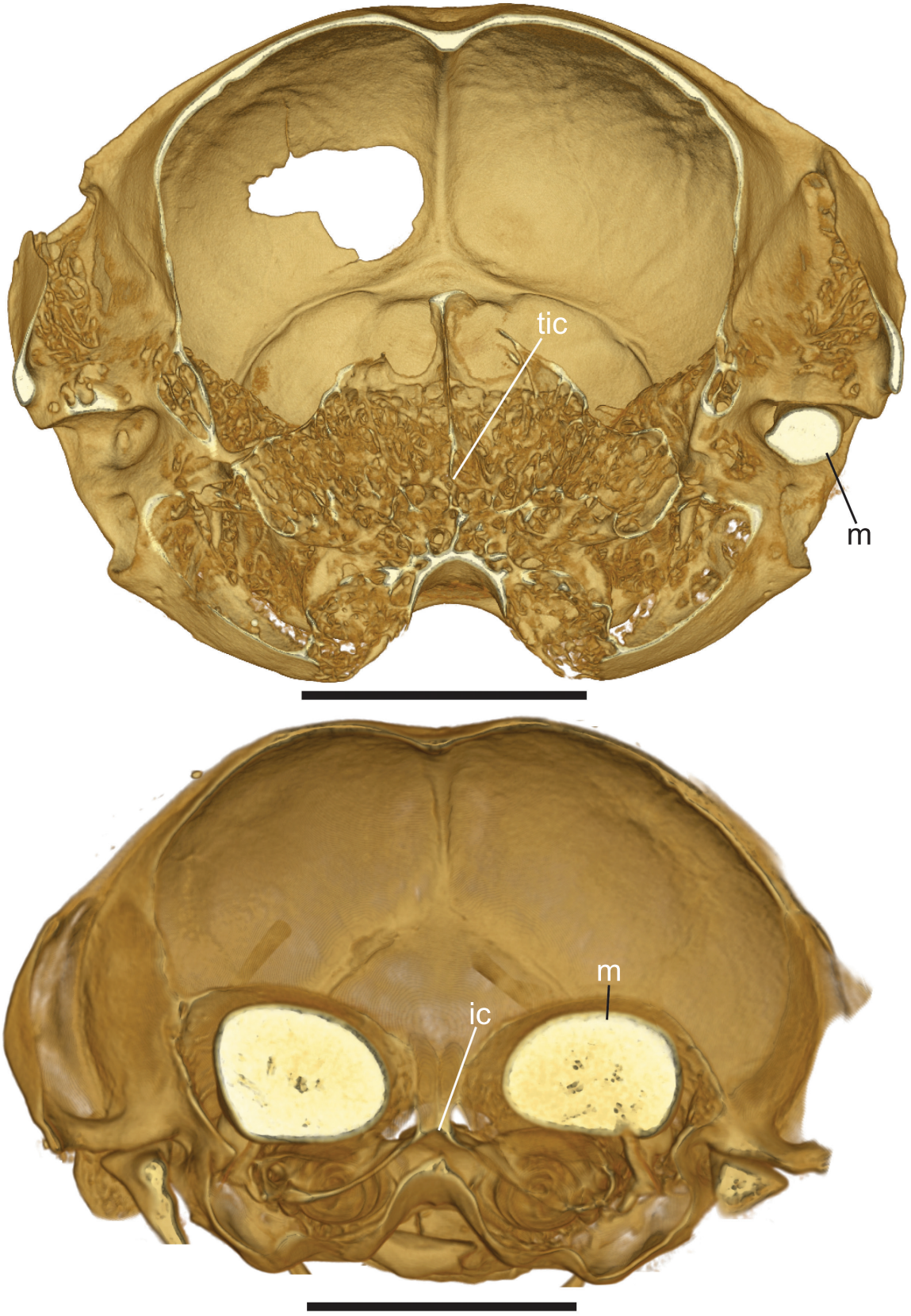

Figure 5. Coronal slices through the posterior skull and ear regions of *Amblysomus hottentotus* (top, ZMB-Mam 35173, previously misidentified as *Calcochloris obtusirostris*) and *Eremitalpa granti* (bottom, NRM-MA 641286). Abbreviations: ic, non-trabeculated interbullar connection; m, malleus; tic, trabeculated interbullar connection. Scale bars: 5 mm.

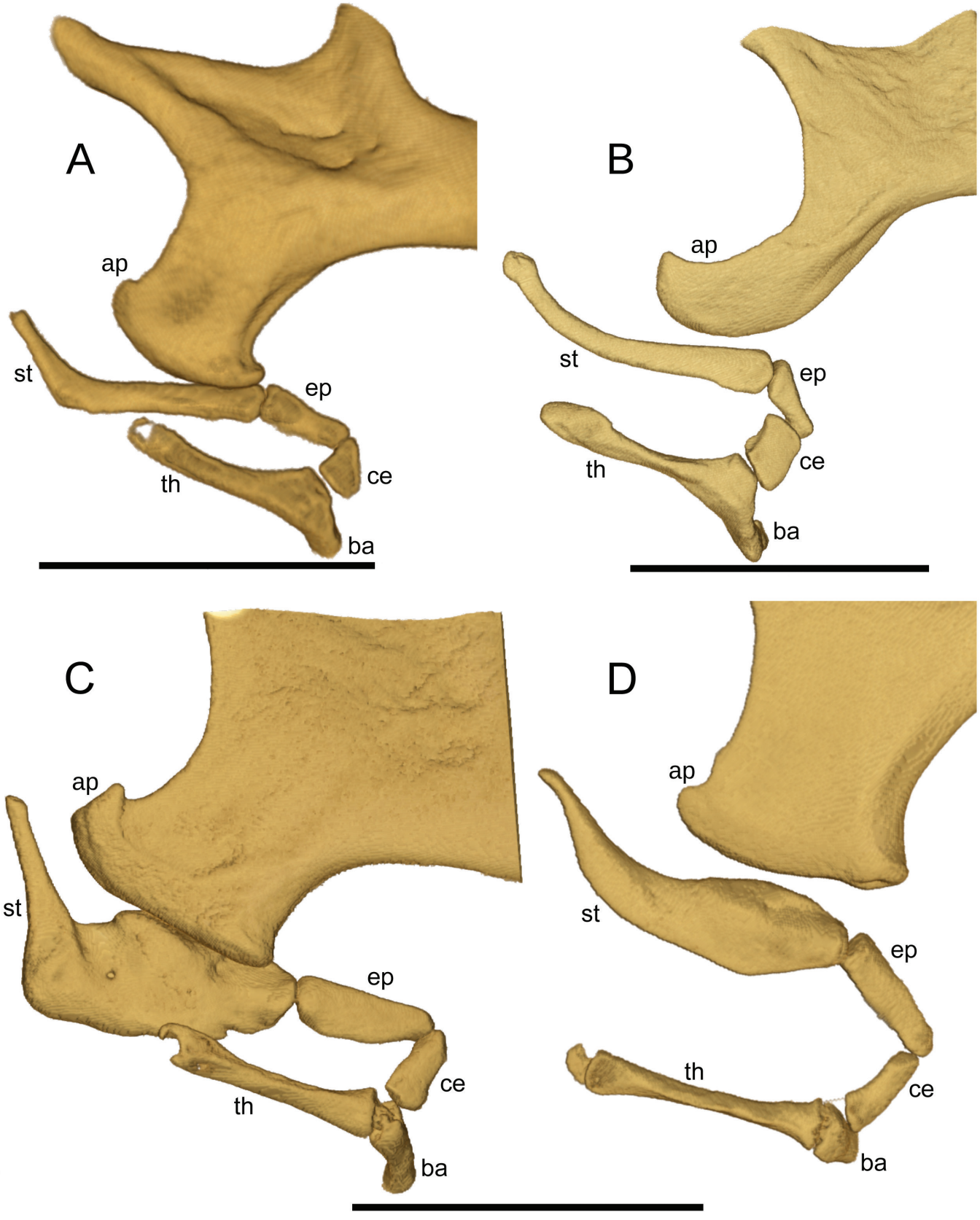

Figure 6. Ventrolateral views of *in situ* right hyoid apparatus and angular process of dentary in *Eremitalpa granti* (A; NRM-MA 641286), *Huetia leucorhinus* (B; AMNH 118829), *Amblysomus meesteri* (C; ZM 42550) and *Chlorotalpa duthieae* (D; ZM 42620). Abbreviations: ap, angular process of dentary; ba, basihyal; ce, ceratohyal; ep, epihyal; st, stylohyal; th, thyrohyal. Scale bars: 5 mm (same for C, D).

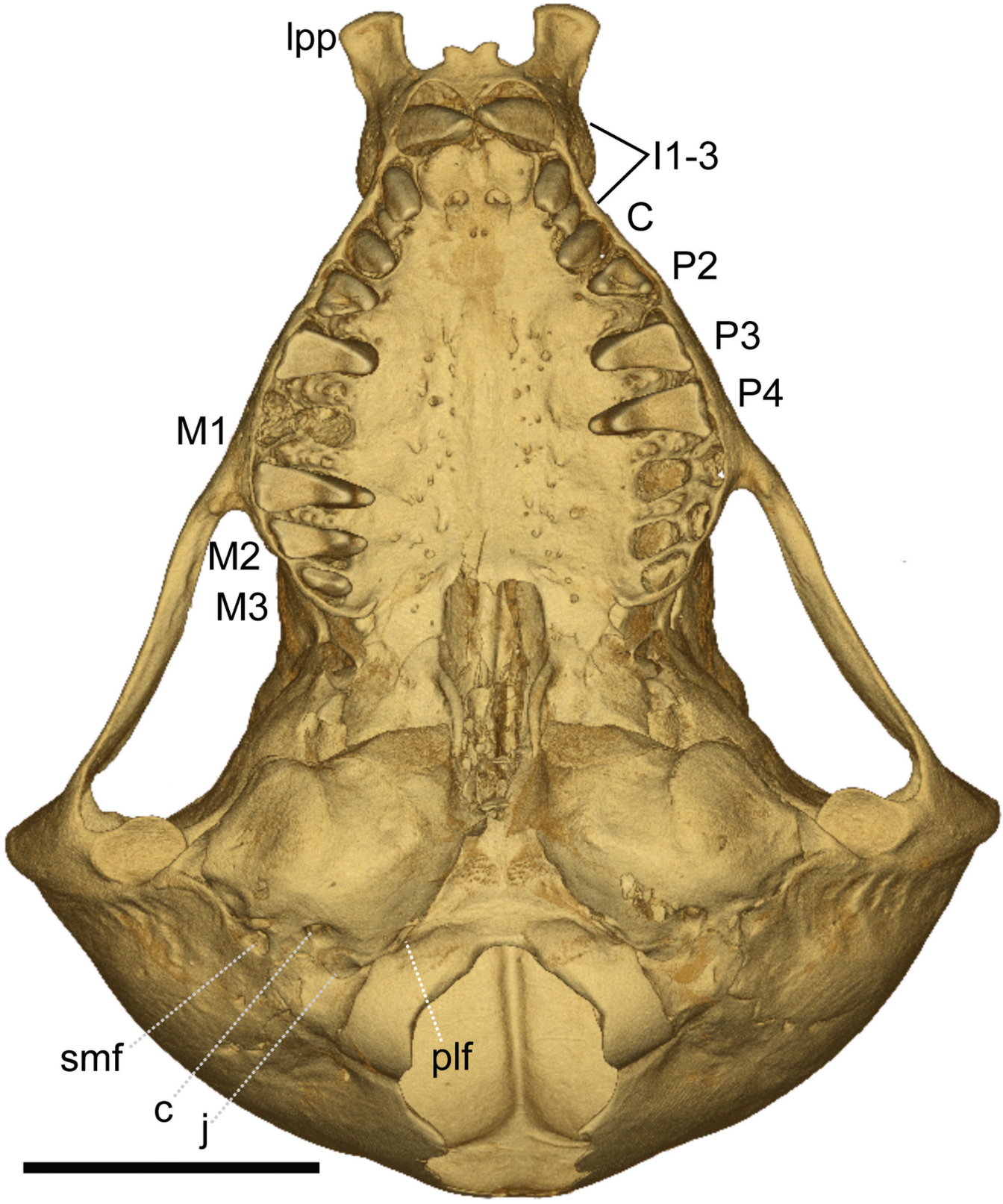

Figure 7. Ventral view of cranium of *Eremitalpa granti* (BMNH 39.472). Dental abbreviations are I, C, P and M for incisors, canine, premolars and molars, respectively. Other abbreviations are c, carotid foramen; j, jugular/posterior lacerate foramen; lpp, lateral process of premaxilla; plf, anterior extension of the posterior lacerate foramen; smf, stylomastoid foramen. Scale bar: 5 mm.

'Chrysochlorinae' is paraphyletic. However, no published investigation has tested these classification schemes with samples of more than one or two genetic loci for most chrysochlorid species. Puttick and Thomas (2015) depicted 18 chrysochlorid species in their figure 1, 14 of which were missing ≥ 90% of their 10.6 kb DNA alignment, and 16 of which lacked morphological

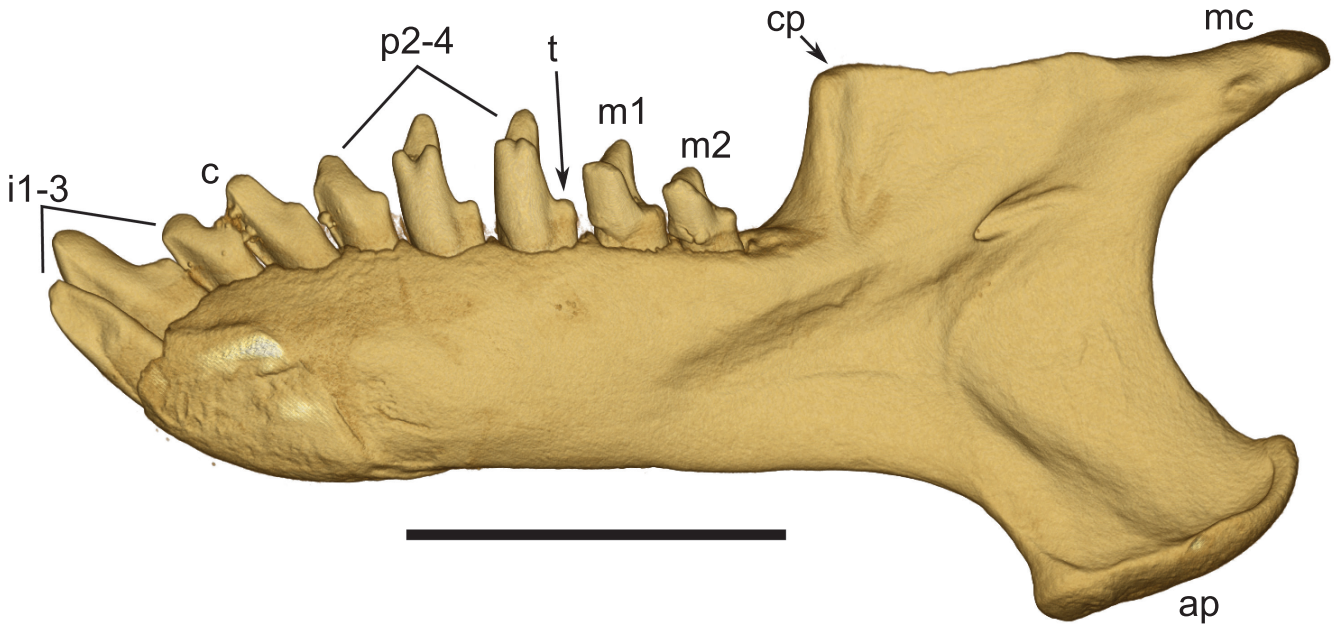

Figure 8. Dentary of *Amblysomus hottentotus* (Asher NFC2) in lingual view. Dental abbreviations given in Figure 7. Other abbreviations are ap, angular process; cp, coronoid process; mc, mandibular condyle; t, talonid cusp. Scale bar: 5 mm.

data. Upham *et al.* (2019) sampled 14 chrysochlorid species along with > 4000 mammalian taxa in a 39 kb alignment, but only two chrysochlorids (*A. hottentotus* and *Chrysochloris asiatica*) contained ≥ 25 kb. *Chrysospalax trevelyani* Günther, 1876 and *Eremitalpa granti* Broom 1907contained 1.7 and 4.6 kb, respectively, and the remaining 10 chrysochlorids in their DNA alignment contained only ~0.8 kb of *GHR* exon 10 (Asher *et al.* 2010). The remaining sites in their alignment for chrysochlorids were unknown, and they determined the placement of seven chrysochlorid terminals in their fig. 1 based on 'taxonomic constraints rather than DNA' (Upham *et al.* 2019: fig. 1 caption).

Fossil golden moles and tenrecs

Neither chrysochlorids nor tenrecids have a particularly good fossil record (Butler 1984, Asher and Seiffert 2010), but it has improved in recent years, particularly with the discovery of remains from Namibia (Pickford 2015a, b, 2018, Mason *et al.* 2017, 2019, Asher 2019). The anatomically best-known fossil chrysochlorid is *Namachloris arenatans* Pickford, 2015a. Originally described as Bartonian (late part of the middle Eocene), but possibly younger (Mason *et al.* 2017; see also Coster *et al.* 2012, Marivaux *et al.* 2014, Sallam and Seiffert 2016, Asher 2019), *Namachloris* exhibits most of the characteristic anatomy of its extant relatives, with a few exceptions. For example, although it shares with certain extant chrysochlorids a trabeculated interbullar region, Mason *et al.* (2017) reported that, unlike most extant species, it lacks a connecting channel between its left and right auditory bullae. It also shows a relatively unenlarged mallear head. Given the morphology of *Namachloris* and the diversity of ossicular morphology within the extant species, it is possible that its morphology represents the generalized ossicular chain that a chrysochlorid ancestor would have had at some point in the evolutionary history of the group, given their shared ancestry with tenrecids and, ultimately, other placental mammals. However, without a clear phylogenetic hypothesis, it remains uncertain if any of the currently known chrysochlorids with small mallear heads represents a plesiomorphic state for the group.

Here, we conduct a phylogenetic analysis that includes multiple genetic loci along with morphological characters for both extant species and fossils. We sampled DNA sequences from three nuclear (*GHR*, *stat5a* and *vWF*) and three mitochondrial (12S rRNA, *cytB* and *ND2*) genes from 35 extant species: 20 chrysochlorids, 13 tenrecids, *Elephantulus* and *Procavia* Storr, 1780 (Table 1). We also sampled morphological data from all these extant taxa plus 13 fossils (Tables 2 and 3), yielding a total of 48 extant and fossil taxa. With this dataset, we test the phylogenetic basis of past classifications of insectivoran-grade afrotherians, in particular those of chrysochlorids based on ossicular anatomy (e.g., Simonetta 1968, Petter 1981). We also tested proposed genus-level affiliations of several species, such as *leucorhinus* and *stuhlmanni*, long suspected of rendering their parent genera (*Calcochloris* and *Chrysochloris*, respectively) paraphyletic.

To better understand the antiquity of the chrysochlorid and tenrecid radiations, we also used a total evidence, Bayesian tip-dating approach (Ronquist *et al.* 2012a), as implemented in MrBayes v.3.2 (Ronquist *et al.* 2012b). This provided a basis upon which to test the age distribution of nodes relevant to key fossils, in particular *Namachloris*, and we combined our molecular and morphological dataset with temporal occurrence information to estimate topology and divergence dates simultaneously. We ultimately seek to illuminate the tempo and mode of character evolution among insectivoran-grade afrotherians and to test the affinities of 13 proposed fossil representatives of extant chrysochlorids and tenrecids.

MATERIALS AND METHODS

Data collection and alignment

We acquired DNA sequences from GenBank, drawing in particular on those generated by Asher *et al.* (2010), Mynhardt

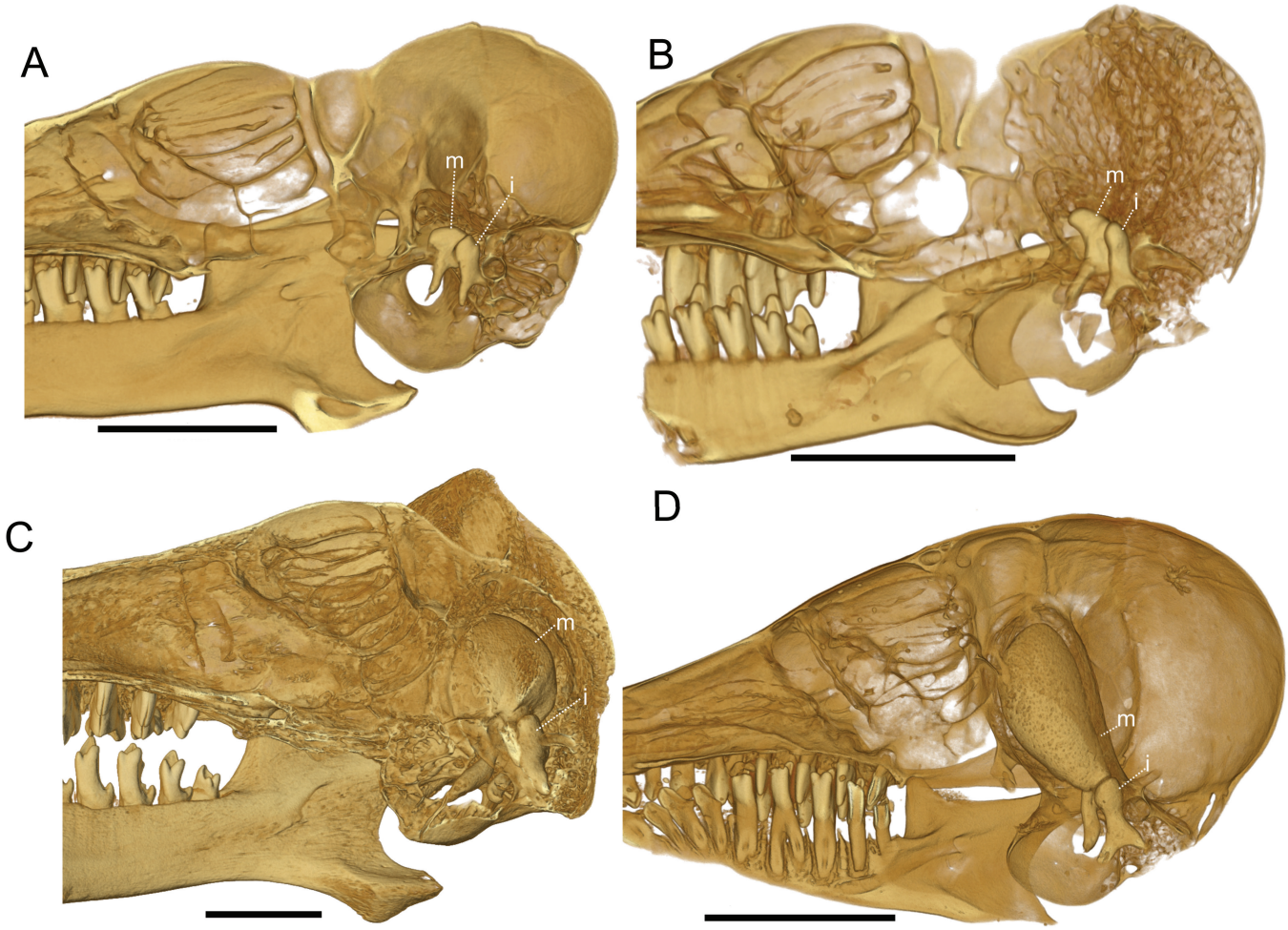

Figure 9. *In situ* right mallei and incudes of *Amblysomus meesteri* (A; ZM 42550), *Huetia leucorhinus* (B; MNHN CG1901-1093), *Chrysospalax trevelyani* (C; UMZC E5470C; image is of left side flipped to appear as right) and *Cryptochloris wintoni* (D; NRM-MA 621447). Abbreviations: i, incus; m, malleus. Scale bars: 5 mm.

et al. (2015) and Everson *et al.* (2016). We also used data from a previously unpublished work (Maree S, Bronner GN, Bennett NC, Oosthuizen CJ, Asher RJ, Hofreiter M, Bloomer P, 2014) and generated new sequences to improve coverage, as shown in Table 1. Methods for DNA extraction and amplification are provided in our Supporting Information (Appendix S1). We used Clustal Omega (https://www.ebi.ac.uk/Tools/msa/clustalo/; Madeira *et al.* 2022) to create initial alignments using default parameters. We then inspected alignments visually with Mesquite (v.3.61; Maddison and Maddison 2019) and performed regional re-alignments with the Opal package (v.2.1; Wheeler and Kececioglu 2007) to preserve reading frames for coding loci and verify sequence homology. Alignments were trivial, except for short regions in our two non-coding genes, 12S rRNA and *stat5a*, which we excluded from the final, concatenated dataset (provided in MrBayes format in Supporting Information, Appendix S2).

Sequences of *stat5a* from *Microgale cowani* Thomas, 1882 (DQ211567) and *Macroscelides proboscideus* Shaw, 1800 (DQ211563) were amplified by Pardini (2006: tables 2.3 and 2.4) using the same primers as two other sequences used in our dataset: *Procavia capensis* (DQ211565) and *Chrysochloris asiatica* (DQ211564). The latter two were easy to align; the former two were not. We therefore excluded *stat5a* for *Microgale cowani* and *Macroscelides proboscideus* from most of our analyses.

We created a separate block of discrete, binary characters representing shared insertions and deletions (indels); these treated contiguous indels as single characters, but we added additional characters for variants of shared length. Indels are named based on the position of the first shared gap prior to the exclusion of alignment-ambiguous regions. After alignment, we deleted isolated leading and trailing sequences and alignment-ambiguous regions, and we treated gaps as missing data. Our concatenated alignment of 5748 aligned sites, 25 indels and 173 morphological characters is available in Supporting Information (Appendix S2).

In all cases, terminal taxa were monophyletic units within our sample. We concatenated molecular and morphological data for each taxon at the species or subspecies level. For example, our DNA and morphological sample of *Eremitalpa granti* derived primarily from the South African subspecies (*Eremitalpa granti granti*) from Pt. Nolloth, except for sequences of *stat5a* derived from a Namibian specimen (*Eremitalpa granti namibiensis* Bauer & Niethammer, 1959; see Table 1). In addition, we joined DNA sequences (12S rRNA, *cytB* and *ND2*) from *Elephantulus edwardii* Smith, 1838 with morphological data and two nuclear

Table 1. GenBank accession numbers for our DNA sample. The Supporting Information (Appendix S1) provides further details on sequences from Maree S, Bronner GN, Bennett NC, Oosthuizen CJ, Asher RJ, Hofreiter M, Bloomer P (2014, unpublished work), shown with 'KM' accession numbers. Bold type indicates new sequences from this study. Novel genus-level attributions since Wilson and Reeder (2005) are *Kilimatalpa* (= '*Chrysochloris*') *stuhlmanni*, *Huetia* (= '*Calcochloris*') *leucorhinus* and *Microgale* (= '*Limnogale*') *mergulus*. Accession numbers in parentheses were used in only a subset of analyses.

Genus	Species	12S	*cytB*	*ND2*	*GHR*	*vWF*	*stat5a*
Procavia	*capensis*	AB096865	AB096865	AB096865	AF392896	U31619	DQ211565
Elephantulus	*edwardii*	NC_041486	NC_041486	NC_041486			
Elephantulus	*rufescens*				AF392876	U31612	
Macroscelides	*proboscideus*						(DQ211563)
Amblysomus	*corriae*	KM388891	KM388913	KM092046	GU904406		KM388951
Amblysomus	*hottentotus*	KM388889	KM388911	KM092008	KT876411	JN415023	KM388949
Amblysomus	*marleyi*	KM388893	KM388915	KM092063	GU904408	KM388936	KM388953
Amblysomus	*meesteri*	KM388892	KM388914	KM092048	KM388970	KM388935	KM388952
Amblysomus	*robustus*	KM388894	KT876424	KM091977	GU904409	KM388937	KM388954
Amblysomus	*septentrionalis*	KM388895	KM388917	KM092061	GU904410	KM388938	KM388955
Calcocholoris	*obtusirostris*	KM388901	KM388926		GU904411	KM388945	KM388962
Carpitalpa	*arendsi*	KM388896	KM388918		GU904413	KM388939	KM388956
Chlorotalpa	*duthieae*	KM388899	KM388921		GU904414	KM388942	KM388959
Chlorotalpa	*sclateri*	KM388900	KM388922	**OR126166**	GU904415		KM388960
Chrysochloris	*asiatica*	KM388902	KM388923	KX015411	GU904416	KM388943	DQ211564
Chrysospalax	*trevelyani*	KM388904	KM388927		AF392877	KM388946	KM388963
Chrysospalax	*villosus*	KM388905	KM388928		GU904418	KM388947	KM388964
Cryptochloris	*wintoni*	**OR147837**	KM388925	**OR126167**	GU904419		
Cryptochloris	*zyli*	KM388903	KM388924	**OR126168**	**OR126169**	KM388944	KM388961
Eremitalpa	*granti*	NC_010304	NC_010304	NC_010304	GU904420		KM388967
Huetia	*leucorhinus*	KM388906	KM388929		GU904412		KM388965
Kilimatalpa	*stuhlmanni*	KM388909	KM388932	KX015412	GU904417	KM388948	KM388968
Neamblysomus	*gunningi*	KM388897	KM388919		GU904421	KM388940	KM388957
Neamblysomus	*julianae*	KM388898	KM388920	KM092024	GU904422	KM388941	KM388958
Echinops	*telfairi*	NC_002631	NC_002631	NC_002631	AF392889	XM_045296004	
Geogale	*aurita*	KX015143		KX015417	DQ202287	KX015382	
Hemicentetes	*semispinosus*	KX015145		KX015420	DQ202288	AJ891093	
Microgale	*cowani*	KX015148		MT188511	KX015327	KX015385	(DQ211567)
Microgale	*dobsoni*	KX015149		KX015424	KX015328	KX015386	
Microgale	*longicaudata*	KX015158		AY193331	KX015337	KX015395	
Microgale	*mergulus*	KX015146		KX015421	DQ202289	AJ891096	
Microgale	*talazaci*	KM388910	KM388933	MK053571	AF392885	KX015404	
Micropotamogale	*lamottei*	KU726981	KU697904	KX015413	DQ202290	AF390538	
Oryzorictes	*tetradactylus*	KX015170		KX015445	KX015326	KX015407	
Potamogale	*velox*	KX015141	OM912806	KX015415	DQ202291		
Setifer	*setosus*	KX015171		KX015446	DQ202292	KX015408	
Tenrec	*ecaudatus*	KX015172		KX015447	AF392890	KX015409	

genes (*GHR* and *vWF*) from *Elephantulus rufescens* Peters, 1878. In a small subset of analyses (not included among our main results), we also joined non-coding, nuclear sequences from *stat5a* from *Macroscelides proboscideus* to make a single terminal, Macroscelididae. This terminal was monophyletic relative to our sample of other afrotherians (Smit *et al.* 2011).

Mynhardt *et al.* (2015) investigated the phylogenetic diversity within the chrysochlorid genus *Amblysomus* and demonstrated the paraphyly of its most geographically widespread species, *A. 'hottentotus'*. To sample a monophyletic terminal for this species, we used only specimens identified from the region in Eastern Cape province where *A. hottentotus* was first described, near King Williams Town and Grahamstown, South Africa. Asher *et al.* (2010) derived *GHR* exon 10 sequences from an *A. hottentotus* specimen (ZMB-Mam 3919; Table 2 contains definitions of 'ZMB' and other institutional abbreviations) collected from a site near Durban, which is unlikely to form a clade with populations of *A. h. hottentotus* from the Eastern Cape (Mynhardt *et al.* 2015). We therefore used another *GHR* exon 10 sequence (KT876411) for this species, derived from the study by Mynhardt *et al.* (2015).

Table 2. Computed tomography (CT) scanned specimens used for coding morphological characters. Museum acronyms are as follows: AMNH, American Museum of Natural History New York; BMNH (also known as NHMUK), Natural History Museum London; FMNH, Field Museum of Natural History Chicago; GSN, Geological Survey of Namibia; IZEA, Institut de Zoologie et d'Ecologie Animale Lausanne; MCZ Museum of Comparative Zoology Harvard; MNHN, Museum National d'Histoire Naturelle Paris; MVZ, Museum of Vertebrate Zoology of the University of California at Berkeley; NHMW, Naturhistorisches Museum Wien; NRM-MA, Naturhistoriska Riksmuseet Stockholm Mammalia; TM, Ditsong (Transvaal) Museum Pretoria; UMMZ, University of Michigan Museum of Zoology; UMZC, University Museum of Zoology Cambridge; YPM, Yale Peabody Museum New Haven; ZM, Iziko South African Museum Cape Town; ZMB-Mam, Museum für Naturkunde Berlin.

Genus	Species	CT scan skull	CT scan skeleton	CT scan body	CT scan head
Procavia	*capensis*	UMZC H5101A	UMZC H5081A, H4981G		
Elephantulus	*edwardii*				
Elephantulus	*rufescens*	ZMB-Mam 75300		MCZ 57173	
Macroscelides	*proboscideus*				
Amblysomus	*corriae*	BMNH 14.11.21.3 and 7.4.7.6		ZM 042553 and ZM 42554	ZM 042553 and ZM 42554
Amblysomus	*hottentotus*	BMNH 47.1399 and 47.1401, NFC2		MCZ 57045	
Amblysomus	*marleyi*				
Amblysomus	*meesteri*			ZM 042550	ZM 042550
Amblysomus	*robustus*			ZM 042549 and ZM 042551	ZM 042549 and ZM 042551
Amblysomus	*septentrionalis*			ZM 42552	ZM 42552
Calcocholoris	*obtusirostris*	BMNH 6.11.8.25 and 6.11.8.26			
Carpitalpa	*arendsi*				
Chlorotalpa	*duthieae*	MNHN 1962-2586		ZM 42547 and ZM 42620	ZM 42547 and ZM 42620
Chlorotalpa	*sclateri*			NHMW 15605	NHMW 15605
Chrysochloris	*asiatica*	AMNH 167961		MVZ 183379, UMZC E5472F	
Chrysospalax	*trevelyani*	UMZC E5470C, AMNH 89040		UMZC 5470D (missing hand and foot)	
Chrysospalax	*villosus*	UMZC E5479A (rostrum and jaws)	UMZC-E5479C (fore- and hind-limb)		
Cryptochloris	*wintoni*			NRM-MA 621447 and 641436	NRM-MA 621447 and 641436
Cryptochloris	*zyli*	MCZ 39628 (rostrum, jaws, stylohyoid, some ear and basicranial elements)	MCZ 39628 (some limb elements in skin)		
Eremitalpa	*granti*	BMNH 47.1383, 39.472		NRM-MA 641286, 641288 and 641289, UMMZ 183384	
Huetia	*leucorhinus*	MNHN CG1901-1083, BMNH 26.7.6.154 and 63.1012, FMNH 81734	NHMW B2742 and FMNH 81734	AMNH 118829	AMNH 118829
Kilimatalpa	*stuhlmanni*	ZMB-Mam 76775		AMNH 82372	AMNH 82372
Neamblysomus	*gunningi*				
Neamblysomus	*julianae*			ZM 42545 and ZM 42546	ZM 42545 and ZM 42546

Table 2. Continued

Genus	Species	CT scan skull	CT scan skeleton	CT scan body	CT scan head
Echinops	*telfairi*	AMNH 170605		YPM 6003	Munich Et97-10
Geogale	*aurita*			UMMZ 167220	
Hemicentetes	*semispinosus*	UMZC E5440I		YPM 5783	
Microgale	*cowani*	UMZC E5459D and E5459B (missing petrosals)	UMZC E5459A	FMNH 237186	
Microgale	*dobsoni*	UMZC E5458B		FMNH 232526	
Microgale	*longicaudata*			UMMZ 174711	
Microgale	*mergulus*			MCZ 45533, FMNH 165440	MCZ 45533, FMNH 165440
Microgale	*talazaci*			FMNH 188741	FMNH 188741
Micropotamogale	*lamottei*				IZEA 1339 and 7083
Oryzorictes	*tetradactylus*	UMZC E5453C	UMZC E5453D		
Potamogale	*velox*	UMZC E5425B	UMZC E5425K and E5425L	UMZC E5425E and E5425F	YPM 14396
Setifer	*setosus*	UMZC 2011.2.2 and 2011.2.6		UMZC 2019.23 and 2019.25	
Tenrec	*ecaudatus*	AMNH 170513		YPM 6029	
Erythrozootes	cf. *chamerpes*	Kampala			
Proamblysomus	*antiquus*	TM uncertain			
Namachloris	*arenatans*	GSN Na1 and Na2			

Publicly available sequences of *vWF* (JN415023) and *GHR* (JN414680) attributed to *A. hottentotus* were derived from specimen 'T1903', tissues of which were given in the 1990s to Mark Springer by John Kirsch, then at the University of Wisconsin Museum of Zoology. We found no further information to identify this specimen to subspecies level. However, BLAST searches on the 743 bp of *GHR* exon 10 accessioned for *A. h. hottentotus* (GenBank accession KT876411), derived from a Ditsong (formerly Transvaal) Museum individual (TM 40051) from Grahamstown by Mynhardt *et al.* (2015), showed greater similarity (99.47%) to the T1903 *Amblysomus GHR* sequences (JN414680) than to those of other *Amblysomus* subspecies, which range in similarity from 97.33 to 99.33%. Other, unpublished sequences from this specimen vary in their similarity to geolocated specimens of *Amblysomus* (Mark Springer, personal communication to R.J.A., 9 June 2023), but we tentatively assumed that sequences derived from T1903 (including *vWF* used here) were attributable to *A. h. hottentotus*. For other *Amblysomus* species, we followed Mynhardt *et al.* (2015) in selecting localities and specimens for each of our terminals.

All DNA and morphological data concatenated for other terminal taxa derived from specimens positively identified to the respective species. Tables 1 and 2 provide the GenBank and museum accession numbers corresponding to each of these terminals.

Morphological data

Our morphological dataset consists of 173 characters in total, most of which are from past matrices (Asher and Hofreiter 2006, Asher *et al.* 2010); six sample chromosomal morphology. Of the hard-tissue characters, 76 are from the skull and hyoid, 37 from the dentition and jaws, and 54 from the postcranial skeleton. The six chromosomal characters are from the literature (Bronner 1995b, Gilbert *et al.* 2006, 2007, 2008) and include the diploid chromosome number for most afrotherian species (Borgaonkar and Gould 1968, Vogel *et al.* 1977, Bronner 1995b, Gilbert *et al.* 2006, 2007, Pardini *et al.* 2007, Gilbert 2008, Smit *et al.* 2011). Other chromosomal characters are more difficult to compare across high-level groups; hence, we focused on five characters known for a subset of chrysochlorids (Gilbert *et al.* 2008: fig. 4).

We list all characters, and illustrate states for our hard-tissue characters, on our morphobank.org project page (see Supporting Information, Appendix S2). Wherever possible, we coded cells using three-dimensional volumes derived from computerized tomographic (CT) scans. We used Drishti v.2.4 and v.3.0 (Limaye 2012, Hu *et al.* 2020) to create volumes and to dissect specimens virtually, and we obtained CT scans for 32 of our 35 extant species and three fossils (Table 2). The three extant taxa missing CT scans (*Amblysomus marleyi* Roberts, 1931, *Carpitalpa arendsi* and *Neamblysomus gunningi* Broom, 1908) were still represented in the matrix of Asher *et al.* (2010); we retained them in our dataset, but acknowledge their correspondingly high frequency of missing data and potential for error.

CT scans of the skulls of three fossils, *Erythrozootes* cf. *chamerpes* Butler & Hopwood 1957, *Proamblysomus antiquus* Broom, 1941 and *Namachloris arenatans*, enabled us to check previous codings for these taxa and to add the latter taxon to our sample. We also relied on our past visits to museum collections

Table 3. Fossil specimens examined. Abbreviations: BMNH (also known as NHMUK), The Natural History Museum London; KNM, National Museums of Kenya Nairobi; L, left; R, right; TM, Ditsong (formerly Transvaal) Museum Pretoria; GSN, Geological Survey of Namibia. For dental abbreviations see the caption for Figure 7. Taxa not listed here were coded based on literature sources (see Materials and methods).

Genus	Species	Institute	Accession number	Material
Erythrozootes	*chamerpes*	BMNH	M21831	L jaw p4–m3
Erythrozootes	*chamerpes*	BMNH	M14314	Rostrum
Erythrozootes	*chamerpes*	KNM	SO17955	R jaw m3, broken m1–m2
Erythrozootes	*chamerpes*	KNM	SO17954	R jaw m3
Erythrozootes	cf. *chamerpes*	Kampala	Uncertain	Skull, basicranium, RM1–RM3, LP2
Protenrec	*tricuspis*	BMNH	M43552	R max P3–M3
Protenrec	*tricuspis*	BMNH	M43551	L jaw p4–m3, roots p3
Protenrec	*tricuspis*	BMNH	M34149	R jaw m1–m2, broken m3
Protenrec	*tricuspis*	BMNH	M34150	L jaw? p3–p4 (or p4–m1?)
Protenrec	*tricuspis*	KNM	LG1490, LG1493	L max P4–M2 (1493) associated with rostrum fragment (1490)
Protenrec	*tricuspis*	KNM	SO1093	L jaw p4–m3
Protenrec	*tricuspis*	KNM	SO1404	R jaw canine root, ?dp2–dp4, m1–m2, erupting p3
Protenrec	*tricuspis*	KNM	SO1417	L max P3–M3
Protenrec	*tricuspis*	KNM	SO1420	R max P2–M3
Protenrec	*tricuspis*	KNM	SO17941	R jaw p3–m1
Parageogale	*aletris*	BMNH	M33046	Rostrum
Parageogale	*aletris*	KNM	CA1548	L max M1–M2
Parageogale	*aletris*	KNM	CA2187	L jaw, talonid
Prochrysochloris	*miocaenicus*	BMNH	M34151	Rostrum
Prochrysochloris	*miocaenicus*	BMNH	M14236	Rostrum
Prochrysochloris	*miocaenicus*	KNM	CA2065	L max P4–M1
Prochrysochloris	*miocaenicus*	KNM	LG63&72	Rostrum
Prochrysochloris	*miocaenicus*	KNM	LG1531	L jaw p4–m3
Prochrysochloris	*miocaenicus*	KNM	LG1552	L max P4, M1, M3
Prochrysochloris	*miocaenicus*	KNM	SO1092	Rostrum, L C–M1
Prochrysochloris	*miocaenicus*	KNM	SO1412	Rostrum, L P4–M3, R P3–M2
Prochrysochloris	*miocaenicus*	KNM	SO1414	R max, P3–M1
Prochrysochloris	*miocaenicus*	KNM	SO17956	Occluding ant max and dent
Prochrysochloris	*miocaenicus*	KNM	SO17957	Ant.skull, RI3–M3, LP2–M3
Namachloris	*arenatans*	GSN	Na1	CT scan Mason *et al.* (2017)
Namachloris	*arenatans*	GSN	Na2	CT scan Mason *et al.* (2017)
Proamblysomus	*antiquus*	TM	1573	Edentulous skull
Proamblysomus	*antiquus*	TM	Uncertain	CT scan Mason *et al.* (2019)
Proamblysomus	*antiquus*	TM	Kromdraai KB 0-6/92	R humerus
Proamblysomus	*antiquus*	TM	Kromdraai KB 0-6/92	R ulna
Proamblysomus	*antiquus*	TM	41559 (Swartkraans mbr 5)	R humerus

and the literature to code these specimens (Tables 2 and 3). Table 2 provides a list of CT scans and Table 3 accession numbers of additional fossil specimens used to help code morphological characters. Table 4 shows the percentage of morphological characters that could be coded for our extant and fossil taxa. Fossils are coded as '?' for all molecular characters.

We also used descriptions in the literature for several species, particularly fossils. These included *Chrysochloris arenosa* and *Chrysochloris bronneri* Asher and Avery 2010, *Namachloris arenatans* (Pickford 2015a, Mason *et al.* 2017), *Proamblysomus antiquus* (Broom 1948b, Asher 2010, Mason *et al.* 2019) and *Prochrysochloris miocaenicus* (Butler and Hopwood 1957, Butler 1984, Mein and Pickford 2003, 2008, Asher 2010).

We sampled isolated humeri, lower jaws, femora and a right ulna from the collections of the Ditsong Museum in Pretoria, derived from the archeological sites Swartkrans members 1 and 5 and Kromdraai. There are at least two chrysochlorid species occurring at these sites: *Chlorotalpa spelea* Broom, 1941 and *Proamblysomus antiquus*. Mason *et al.* (2019) described what is most probably the skull from Kromdraai described by Broom (1941) and also mentioned by De Graaff (1958). What DeGraaff described as '*Chrysotricha*' *hamiltoni* ('*Amblysomus*' following Butler 1978) from Sterkfontein is another potential species to which these postcranial elements might belong. Whatever the association is, the elements all show the same states for the morphological characters we sampled. The only taxon from

Table 4. Proportion of missing data in morphological dataset

Taxon	Terminal	Percentage missing
Hyracoidea	*Procavia capensis*	3
Macroscelididae	*Elephantulus*	3
Chrysochloridae	*Amblysomus corriae*	4
Chrysochloridae	*Amblysomus hottentotus*	3
Chrysochloridae	*Amblysomus marleyi*	46
Chrysochloridae	*Amblysomus meesteri*	4
Chrysochloridae	*Amblysomus robustus*	3
Chrysochloridae	*Amblysomus septentrionalis*	7
Chrysochloridae	*Calcochloris obtusirostris*	14
Chrysochloridae	*Carpitalpa arendsi*	21
Chrysochloridae	*Chlorotalpa duthieae*	6
Chrysochloridae	*Chlorotalpa sclateri*	6
Chrysochloridae	*Chrysochloris asiatica*	2
Chrysochloridae	*Chrysospalax trevelyani*	7
Chrysochloridae	*Chrysospalax villosus*	13
Chrysochloridae	*Cryptochloris wintoni*	7
Chrysochloridae	*Cryptochloris zyli*	30
Chrysochloridae	*Huetia leucorhinus*	5
Chrysochloridae	*Kilimatalpa stuhlmanni*	6
Chrysochloridae	*Eremitalpa granti*	3
Chrysochloridae	*Neamblysomus gunningi*	13
Chrysochloridae	*Neamblysomus julianae*	3
Tenrecidae	*Geogale aurita*	3
Tenrecidae	*Echinops telfairi*	3
Tenrecidae	*Hemicentetes semispinosus*	3
Tenrecidae	*Microgale cowani*	3
Tenrecidae	*Microgale dobsoni*	7
Tenrecidae	*Microgale longicaudatus*	10
Tenrecidae	*Microgale mergulus*	4
Tenrecidae	*Microgale talazaci*	6
Tenrecidae	*Micropotamogale lamottei*	14
Tenrecidae	*Oryzorictes tetradactulus*	8
Tenrecidae	*Potamogale velox*	4
Tenrecidae	*Setifer setosus*	3
Tenrecidae	*Tenrec ecaudatus*	3
Fossil	*Arenagale calcareus*	88
Fossil	*Chrysochloris arenosa*	56
Fossil	*Chrysochloris bronneri*	88
Fossil	*Erythrozootes chamerpes*	58
Fossil	*Namachloris arenatans*	32
Fossil	*Nanogale fragilis*	93
Fossil	*Namagale grandis*	80
Fossil	*Parageogale aletris*	87
Fossil	*Proamblysomus antiquus*	69
Fossil	*Prochrysochloris miocaenicus*	74
Fossil	*Promicrogale namibiensis*	95
Fossil	*Protenrec tricuspis*	80
Fossil	*Sperrgale minutus*	86

these South African cave sites in our sample is *Proamblysomus antiquus*, and we assumed their association with the craniodental material we have from this species.

Fossil tenrecids in our sample included *Arenagale calcareus* (Pickford 2015b), *Erythrozootes chamerpes* (Butler and Hopwood 1957, Butler 1984, Asher and Hofreiter 2006, Asher 2010), *Namagale grandis* (Pickford 2015b), *Nanogale fragilis* (Pickford 2019), *Parageogale aletris* (Butler and Hopwood 1957, Butler 1984, Asher and Hofreiter 2006, Asher 2010), *Promicrogale namibiensis* (Pickford 2018), *Protenrec tricuspis* (Butler and Hopwood 1957, Butler 1984, Mein and Pickford 2003, 2008, Asher and Hofreiter 2006, Asher 2010) and *Sperrgale minutus* (Pickford 2015b).

All the fossils in our taxon sample were missing at least some data. The most complete was *Namachloris arenatans* (Pickford 2015a, Mason *et al.* 2017), missing 32% of its 173 morphological characters. The next most-complete taxa were *Chrysochloris arenosa* (Asher and Avery 2010) and *Erythrozootes chamerpes* (Butler 1984, Asher 2010) missing 56% and 58%, respectively, of their morphological characters. The remaining fossils ranged from 69% (*Proamblysomus antiquus*) to 95% (*Promicrogale namibiensis*) missing data (Table 4).

Model selection and phylogenetic search criteria

After defining codon positions for our four protein-coding loci (*cytB*, *ND2*, *GHR* and *vWF*), we used PartitionFinder 2 (Lanfear *et al.* 2012, 2016) to test among the models of sequence evolution available in MrBayes (v.3.2; Ronquist *et al.* 2012b) using a greedy search arbitrated by two information-theoretic scores: the Bayesian information criterion (BIC) and the corrected Akaike information criterion (AICc; see Table 5). We treated our morphological characters as a discrete partition using the 'standard discrete' model with gamma-distributed rate variation ('lset … rates=gamma') and assumed inclusion of variable characters ('lset … coding=variable') for morphological and indel characters.

Our Bayesian analyses entailed eight runs with four chains each, with at least six million generations, sampling every 2000th. We used the MPI version of MrBayes v.3.2 on the University of Cambridge High Performance Computing cluster and discarded the first 25% of runs as burn-in. We explored burn-in values using Tracer v.1.7 (Rambaut *et al.* 2018) to ensure that our analyses converged, based on estimates of effective sample size well over 1000 for the log-likelihood of our combined runs, a standard deviation of split frequencies ≤ .02, and a potential scale reduction factor (PSRF) within .01 of one for all parameters. Optimal topologies, branch lengths and posterior probabilities (pp) are derived from a majority rule consensus across post-burn-in trees from all runs.

For our maximum parsimony (MP) analyses, we used TNT (v.1.5; Goloboff *et al.* 2008, Goloboff and Catalano 2016) and explored equal and implied weighting constants (Goloboff 1993). We chose an implied weighting value that maximized congruence with the tenrecid topology figured by Everson *et al.* (2016: fig. 3). To visualize topologies, we used FigTree v.1.4.4 (Rambaut 2018).

Timetree analysis

We assigned uniform priors according to age uncertainty in the form of upper and lower occurrence dates for fossil tip calibrations. Where possible, we used narrow priors: 5–6.5 Myr for *Chrysochloris arenosa* and *Chrysochloris bronneri*; .5–4.5 Myr for *Proamblysomus antiquus*; and 19–21 Myr for *Erythrozootes*

Table 5. Models of sequence evolution identified by PartitionFinder2 (Lanfear *et al.* 2016) and their corresponding molecular partition. BIC, Bayesian Information Criterion, AICc, corrected Akaike Information Criterion

Criterion	Subset	Model	# sites	Partition names
BIC	1	GTR+I+G	1482	cytbfst, rna
BIC	2	HKY+G	1036	cytbsnd, ghrsnd, vwfsnd
BIC	3	HKY+I+G	380	cytbtrd
BIC	4	GTR+I+G	348	NDfst
BIC	5	GTR+I+G	348	NDsnd
BIC	6	HKY+I+G	348	NDtrd
BIC	7	K80+G	781	ghrtrd, stat
BIC	8	HKY+G	655	ghrfst, vwffst
BIC	9	GTR+G	370	vwftrd
AICc	1	GTR+G	380	cytbfst
AICc	2	HKY+I+G	380	cytbsnd
AICc	3	GTR+I+G	380	cytbtrd
AICc	4	GTR+I+G	348	NDfst
AICc	5	GTR+I+G	348	NDsnd
AICc	6	GTR+I+G	348	NDtrd
AICc	7	GTR+G	656	ghrsnd, vwfsnd
AICc	8	GTR+G	286	ghrtrd
AICc	9	GTR+G	655	ghrfst, vwffst
AICc	10	GTR+G	370	vwftrd
AICc	11	HKY+G	495	stat
AICc	12	GTR+I+G	1102	rna

chamerpes, *Parageogale aletris*, *Prochrysochloris miocaenicus*, *Promicrogale namibiensis* and *Protenrec tricuspis*. As the age of Eocliff fossils is disputed, we followed Sallam and Seiffert (2016) and set a broad, uninformative prior of 20–47 Myr that covers the middle Eocene to earliest Miocene, which includes estimates of Lutetian and Bartonian, as proposed by Pickford *et al.* (2014) and Pickford (2015a), respectively. In so doing, we estimated tip ages of these fossils based on their anatomy, given the morphological clock (Ronquist *et al.* 2012a).

To test the impact of the age prior for Eocliff fossils on other nodes, we also ran the analysis with narrow priors (20–30 Myr), using the inferred age of Eocliff fossils from our analysis with broad priors (see Results). For the Black Crow locality (Pickford *et al.* 2014, Van Couvering and Delson 2020), we set the uniform prior of *Nanogale fragilis* to 37–59 Myr. The ages of extant taxa were fixed to zero.

Alignments, partitions and models were the same as in the BIC non-clock analysis (Table 5). We derived a suitable clock rate prior from path lengths of the non-clock MrBayes tree, and the mean age of the fossil tips using an R script from Gunnell *et al.* (2018). This test suggested a lognormal distribution (mean = −4.43118, SD = .27458) as a good starting point for the clock rate. We used the independent gamma rates (IGR) model to estimate relaxed clock rate variation, and a fossilized birth–death prior on branch lengths with a speciation prior ('speciationpr') of exp(10) and flat priors for extinction ('extinctionpr') and fossilization ('fossilizationpr') priors. We set the sampling probability of terminal lineages ('sampleprob') to .4, because our sample of 35 extant species composes 40% of the ~87 extant afrotherian species. We used an exponential prior with offset for root age, with a mean of 80 Myr (Upham *et al.* 2019) and a minimum offset of 61 Myr, based on the lower bound for *Eritherium azzouzorum* Gheerbrant et al., 2012, the oldest unambiguous crown afrotherian. This means that the afrotherian root will be older than 61 Mya (as per the age of *Eritherium*) but very probably younger than 80 Mya, consistent with the range proposed by Alvarez-Carretero *et al.* (2022: fig. 3). We ran two Markov chain Monte Carlo chains with four runs each for 10 million generations, sampling every 1000 generations, and discarded the first 25% as burn-in. We summarized trees with 'sumt contype=allcompat' and extracted the distribution of relevant tip and node ages from the post-burn-in, posterior tree sample using the 'obtainDatedPosteriorTreesMrB()' and 'dateNodes()' functions of the paleotree package (Bapst 2012) in R v.4.0.3 (R Core Team 2020). We calculated posterior probabilities for the timetree analysis by integrating their density over all possible parameter models. This density is the product of the likelihood of the tree and the prior probability density of the tree and model divided by the probability of the data. Thus, posterior probabilities in our timetree analysis account for probability of branch length in time units.

RESULTS

Optimal topologies resulting from Bayesian and parsimony analyses of the extant taxa sampled for DNA and morphology share several features in common. Nearly all nodes in the analyses of extant taxa are bifurcating, and most show Bayesian posterior probabilities of 1.0 (Figs 10A, 11A), although these decline substantially with the inclusion of fossil taxa (Fig. 12; Supporting Information Fig. S1).

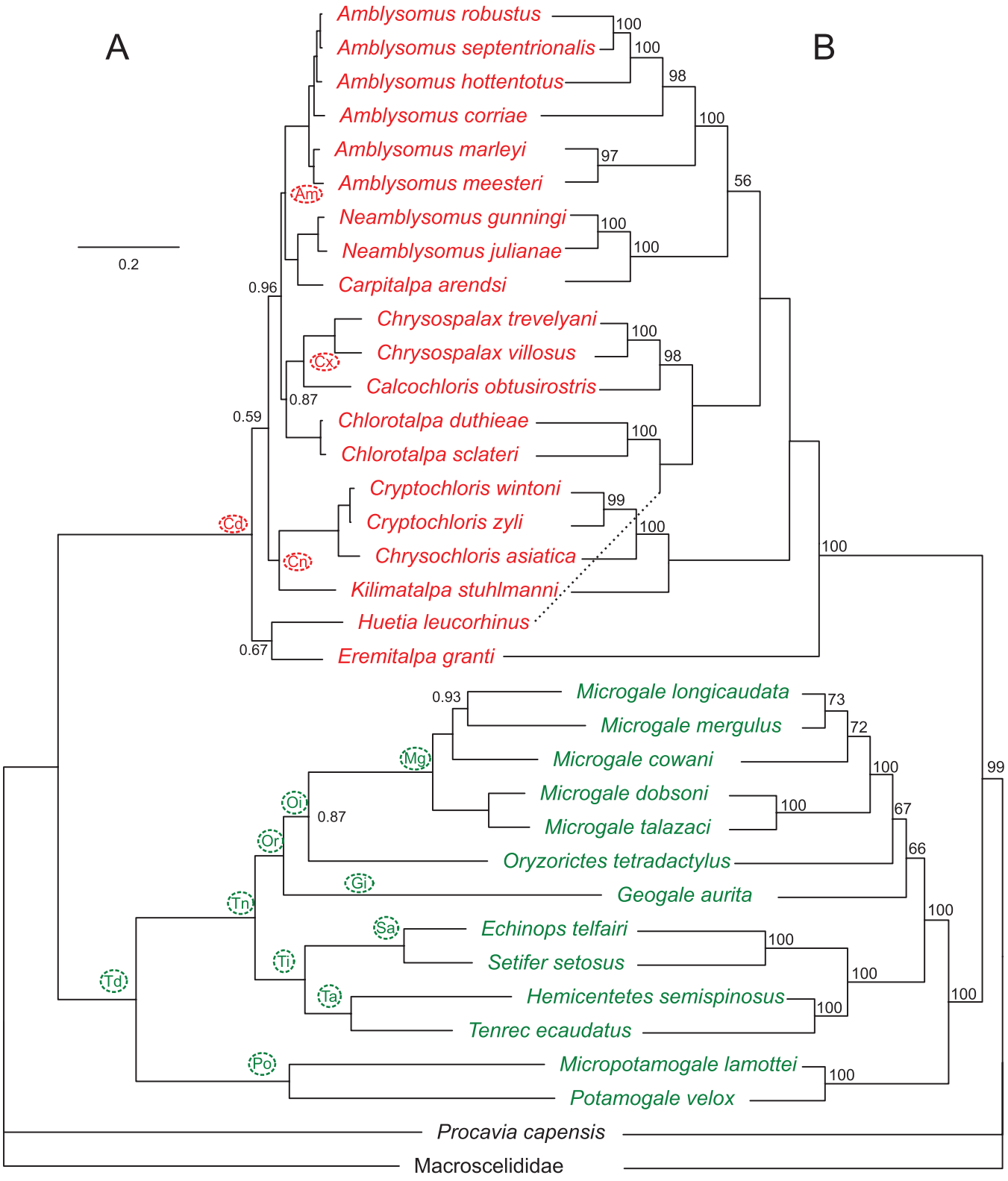

Figure 10. Topologies resulting from Bayesian-BIC (A, left) and parsimony implied weighting $K = 4$ (B, right) analyses of extant taxa sampled for six genes (*cytB*, *ND2*, *GHR*, *vWF*, 12S and *statSa*) and indels. Bayesian branch lengths reflect the scale at the top left; parsimony branch lengths are arbitrary. Only chrysochlorids and *Procavia* are known for *statSa* (for other missing loci, see Table 1). Bayesian nodes have a posterior probability of one unless indicated otherwise. Numbers adjacent to parsimony nodes represent bootstrap values, calculated with 500 pseudoreplicates of a TNT search using mult = tbr 100 replicates each and reported only at or over 50. Chrysochlorids are in red, tenrecids green. Circled and coloured letters adjacent to nodes indicate high-level taxonomy: Am, Amblysominae; Cd, Chrysochloridae; Cn, Chrysochlorinae; Cx, Chrysospalacinae; Gi, Geogalini; Mg, *Microgale*; Oi, Oryzorictini; Or, Oryzorictinae; Po, Potamogalinae; Sa, Setiferina; Ta, Tenrecina; Td, Tenrecidae; Tn, Tenrecinae; Ti, Tenrecini.

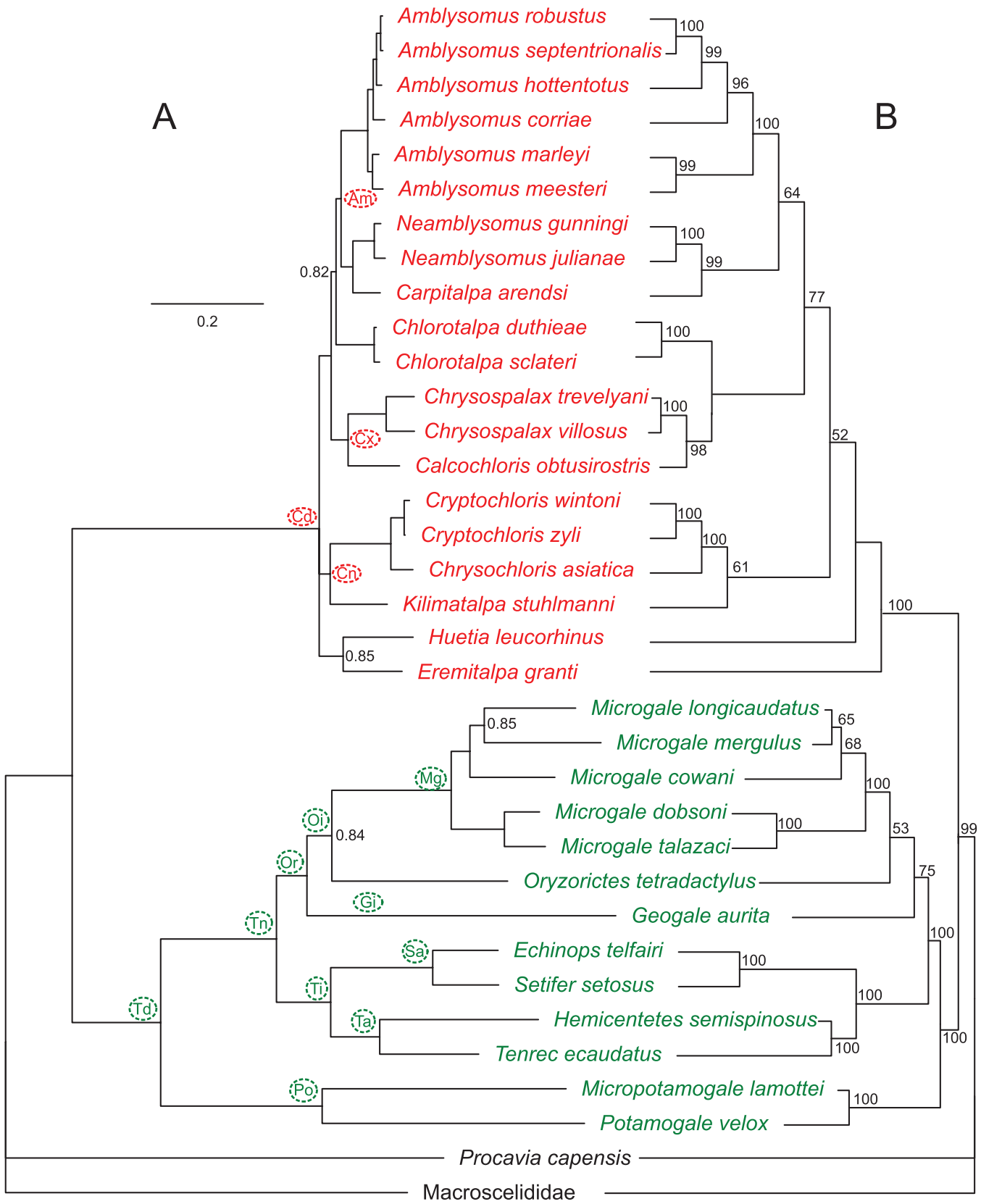

Figure 11. Topologies resulting from Bayesian-BIC (A; left) and parsimony implied weighting $K = 4$ (B; right) analyses of extant taxa sampled for six genes (*cytB*, *ND2*, *GHR*, *vWF*, 12S and *statSa*), indels and morphology. Branch lengths reflect the scale at the top left; parsimony branch lengths are arbitrary. Only chrysochlorids and *Procavia* are known for *statSa* (for other missing loci, see Table 1). Bayesian nodes have a posterior probability of one unless indicated otherwise. Numbers adjacent to parsimony nodes represent bootstrap values, calculated with 500 pseudoreplicates of a TNT search using mult = tbr 100 replicates each and reported only at or over 50. Chrysochlorids are red, tenrecids green. Circled and coloured letters adjacent to nodes indicate high-level taxonomy, as shown in Figure 10.

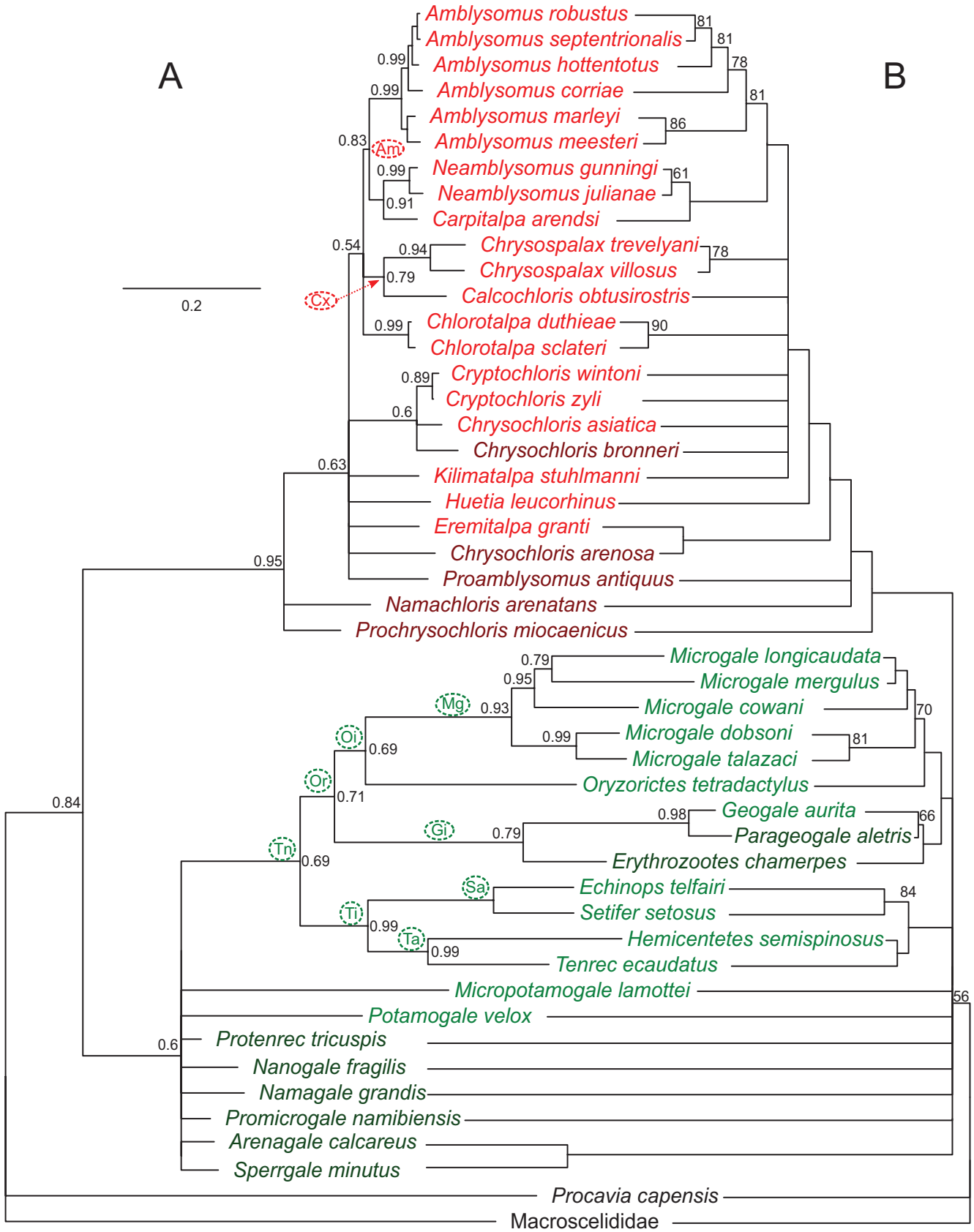

Figure 12. Topologies resulting from Bayesian-BIC (A; left) and parsimony implied weighting $K = 4$ (B; right) analyses of extant taxa sampled for six genes (*cytB*, *ND2*, *GHR*, *vWF*, 12S and *statSa*) and indels, plus fossils and morphological data sampled for all. Bayesian branch lengths reflect the scale at the top left; parsimony branch lengths are arbitrary. Only chrysochlorids and *Procavia* are known for *statSa* (and other regions of missing data are shown in Table 1). Bayesian nodes have a posterior probability of one unless indicated otherwise. Numbers adjacent to parsimony nodes represent bootstrap values, calculated with 250 pseudoreplicates of a TNT search using mult = tbr 10 replicates each and reported only at or over 50. Chrysochlorids are red, tenrecids green; fossils are darker shades of each. Circled and coloured letters adjacent to nodes indicate high-level taxonomy, as shown in Figure 10.

In addition, a few key nodes including the root are inconsistently resolved and/or exhibit much lower support indices (Fig. 12). In general, branch lengths among chrysochlorids are much shorter than those for tenrecids (Figs 10A, 11A), indicating that more data are needed to resolve certain areas of the tree confidently.

The dataset for tenrecs used by Everson *et al.* (2016) consisted of four mitochondrial and eight nuclear loci, most of which remain unknown for chrysochlorids. Nonetheless, and given that we sampled fewer species of *Microgale* Thomas, 1882, our optimal Bayesian analyses of extant taxa (Figs 10A, 11A) were consistent with their optimal topology for tenrecs (Everson *et al.* 2016: fig. 3). For our parsimony analyses of extant taxa (Figs 10B, 11B), an implied weighting constant of $K = 4$ resulted in a topology consistent with Everson *et al.* (2016: fig. 3).

Tenrecidae

Our results for tenrecids at the Linnean rank of family and below are generally consistent with the taxonomy used by Bronner and Jenkins (2005) and Asher and Helgen (2010). This supports division of tenrecids into monophyletic potamogalines and tenrecines, the web-footed tenrec (*Microgale mergulus* Major, 1896) as part of the genus *Microgale* (as first proposed by Olson and Goodman 2003), a *Microgale dobsoni* Thomas, 1884–*Microgale talazaci* Major, 1896 clade as sister taxon to all other species of *Microgale*, and an *Oryzorictes* Grandidier, 1870–*Microgale* clade, which we call Oryzorictini. This clade comprises the sister taxon of *Geogale aurita* Milne-Edwards & Grandidier, 1871 and collectively forms the Oryzorictinae (Figs 10, 11). The taxon Geogalini is available to encompass fossil species more closely related to *G. aurita* than to other tenrecids, such as the fossil taxa *Parageogale* and *Erythrozootes* (Fig. 12). Tenrecini consists of *Setifer* Froriep, 1806–*Echinops* Martin, 1838 (Setiferina) and *Tenrec* Lacépède, 1799–*Hemicentetes* Mivart, 1871 (Tenrecina) and is collectively the sister taxon to all other extant Malagasy tenrecs in the Oryzorictinae (i.e., geogalins plus oryzorictins).

Our equally weighted parsimony analysis diverged from Everson *et al.* (2016: fig. 3) in reconstructing *Mi. mergulus* as sister to a *Mi. dobsoni–Mi. talazaci* clade and in placing *G. aurita* as sister to Tenrecini rather than Oryzorictinae. We regard these signals as artefacts and instead draw our conclusions based on the Bayesian (Figs 10A, 11A, 12A; Supporting Information, Fig. S1) and implied-weighting (Figs 10B, 11B, 12B) topologies.

Chrysochloridae

Our analyses of extant taxa (Figs 10, 11) strongly support the placement of *Calcochloris obtusirostris* as the sister taxon of the two species of *Chrysospalax*, *Chrysospalax trevelyani* and *Chrysospalax villosus* Smith, 1833. They also support *Carpitalpa arendsi* as the sister taxon to *Neamblysomus*, a clade which, in turn, forms the sister taxon to *Amblysomus*. The species *stuhlmanni*, long regarded as part of the genus *Chrysochloris* (Bronner and Jenkins 2005), appears instead as sister taxon to a *Chrysochloris asiatica–Cryptochloris* clade. We therefore elevate *Kilimatalpa* (Lundholm 1954) from subgeneric to generic status, leaving both generic names monotypic for extant species, in reference to *Kilimatalpa stuhlmanni* and *Chrysochloris asiatica*.

Based on these results, we define the Amblysominae as the group encompassing *Amblysomus* and its sister taxon *Neamblysomus–Carpitalpa arendsi* (Figs 10, 11). Our data also support the intrageneric relationships of *Amblysomus* as articulated by Mynhardt *et al.* (2015), in particular that the species *marleyi* and *meesteri* Bronner, 2000, previously regarded as subspecies of *A. 'hottentotus'*, comprise the sister clade to all other species of *Amblysomus*. This is also consistent with the treatment of *marleyi* as a separate species of *Amblysomus* by Bronner (1995a, 2000). As in the study by Mynhardt *et al.* (2015), our data place *Amblysomus corriae* Thomas, 1905, the only species of *Amblysomus* broadly distributed throughout the Western Cape province of South Africa, as the sister taxon to the remaining non-*meesteri*/*marleyi* species of *Amblysomus*. Our data do not address the phylogeography of *A. 'hottentotus'* populations outside of the Eastern Cape, but are also consistent with Mynhardt *et al.* (2015) by placing *A. septentrionalis–A. robustus* as the most-nested clade within the genus, sister to *A. h. hottentotus sensu stricto* (i.e., populations near Grahamstown and King Williams Town in the Eastern Cape).

The two information-theoretic criteria (BIC vs. AICc; see Table 5) we used to derive models of sequence evolution resulted in mutually consistent topologies except for the chrysochlorid root node. The BIC topology based on DNA–indels–morphology showed a trichotomy (Fig. 11A); the AICc topology placed a *Kilimatalpa–Chrysochloris–Cryptochloris* group (pp = 1.0) diverging from a clade containing the remaining extant chrysochlorids (pp = .56). Using only DNA–indels, BIC favoured a divergence of *Eremitalpa–Huetia* (pp = .67) from a clade containing other extant chrysochlorids (pp = .59; Fig. 10A), whereas AICc showed a trichotomy. Neither BIC nor AICc Bayesian analyses including our fossil taxa resolved the root of crown Chrysochloridae, but both reconstructed *Namachloris* and *Prochrysochloris* on the chrysochlorid stem (Fig. 12A; Supporting Information, Fig. S1).

Besides the ambiguity surrounding the extant chrysochlorid root, and using either BIC or AICc for model selection, adding morphology to our DNA–indel alignment led to one topological difference: the placement of *Chlorotalpa* as sister to amblysomines (pp = .92; Fig. 11A) rather than *Chrysospalax–Calcochloris* (pp = .87; Fig. 10A). Parsimony with implied weights favoured the latter (*Chlorotalpa*, (*Chrysospalax*, *Calcochloris*)), with the further complication that without morphology, *Huetia* was also drawn into a clade with *Chlorotalpa* (Fig. 10B), albeit with bootstrap support < 50%. In contrast, the optimal parsimony topology using implied weights with DNA–indels–morphology reconstructed *Huetia* near the base of the chrysochlorid crown radiation, one node crownward from *Eremitalpa* with parsimony bootstrap support of 61% (Fig. 11B).

While our dataset does not resolve the chrysochlorid root node, it does narrow down the possibilities to a subset of the species previously included in the 'Chrysochlorinae' (Bronner and Jenkins 2005), rendering that taxon paraphyletic. We therefore restrict the taxon Chrysochlorinae to the smaller clade of *Kilimatalpa* as sister taxon to *Chrysochloris asiatica–Cryptochloris* (Bayesian pp = 1.0). We propose the designation Chrysospalacinae for *Calcochloris obtusirostris–Chrysospalax* (Figs 10, 11). The affinities of the remaining three chrysochlorid genera, *Chlorotalpa* (restricted here to *Chlorotalpa sclateri* and *Chlorotalpa duthieae*),

Eremitalpa and *Huetia*, are not yet resolved with sufficient support to merit high-level taxonomic designations.

Fossil tenrecs and golden moles

In general, our morphological dataset allows for only a few generalizations concerning the fossil relatives of insectivoran-grade afrotheres. The assignment of fossils into one or the other group is consistent with the literature, in particular that *Namachloris* is a stem chrysochlorid, outside the radiation of the crown group (cf. Pickford 2015a, Mason *et al.* 2017). *Prochrysochloris miocaenicus* (Butler and Hopwood 1957, Butler 1984, Asher 2010) is also reconstructed outside of the crown, as is *Proamblysomus* (Broom 1941, 1948b, Mason *et al.* 2019) according to parsimony (Fig. 12B) but not our Bayesian topologies (Fig. 12A; Supporting Information, Fig. S1), in which it is unresolved.

Namachloris is the best-known chrysochlorid fossil, and we agree with the analyses of Pickford (2015a) and Mason *et al.* (2017) that it comprises the sister taxon of extant golden moles. It is more closely related to chrysochlorids than to other taxa in our sample but shows important differences. Mason *et al.* (2017) noted the lack of an interbullar connection (character 7) and the convergence of this feature to only one extant species, *Chrysospalax villosus*. (We provide illustrations for this and other morphological characters on our morphobank site, as indicated in Supporting Information, Appendix S2.) *Namachloris* also exhibits a less derived ossicular chain, with an ovoid rather than rectangular or hyper-elongated incus (character 14) and an inferior stapedial foramen separate from the foramen ovale (character 18). We also note that its jugular foramina are not situated immediately dorsal to each occipital condyle, as in extant species, but more anterior and dorsal, as in most small mammals (character 23). The origin of the maxillary root of its zygoma is lateral to M2, as in most tenrecids, rather than to M1 or further anteriorly, as in other chrysochlorids (character 53). *Namachloris* shows a slightly wider interpterygoid region relative to its palatal width (character 65), similar to many tenrecids and less common (but not unheard of, e.g., *Chrysospalax*) among chrysochlorids. The angular process of the dentary as figured by Pickford (2015a: figs 12, 19) is narrower relative to dentary length (character 68) than in most other chrysochlorids, resembling *Huetia* and, to a lesser extent, *Eremitalpa*, but not other crown species. *Namachloris* also shows relatively narrow upper (character 87) and lower (character 101) third premolars, has a connate metacone (character 89), a large upper molar protocone (character 90), an anteriorly projecting M1 parastyle (character 92), a buccolingually wide M3 (character 97) and a mesiodistally unreduced third lower molar (character 108), again resembling certain tenrecids.

While no information is yet forthcoming about the anatomy of the *Namachloris* hyoid apparatus, the shape of its dentary angular process provides some clues. Pickford (2015a: fig. 12) shows an intact angular process of the dentary in *GSN-Na1*, which is missing in the CT scan we have of the same specimen. Using the scale provided by Pickford (2015a: fig. 12), the ventral margin of the angular process in GSN-Na1 is likely to be between 1.0 and 1.4 mm in anteroposterior length. Another specimen (GSN-Na34; Pickford 2015a: fig. 19) shows an intact angular process measuring ~1.9 mm. Accounting for the relative differences in size among *Namachloris* specimens GSN-Na1, GSN-Na2 and GSN-Na34, angular process length shows a range from 8 to 11% of dentary length in *Namachloris*. This is shorter than in any extant chrysochlorid but approaches the lower range of *Eremitalpa* (13–20%) and *Huetia* (14%). The longest angular processes are evident in specimens of *A. hottentotus*, *Chrysochloris asiatica* and *Neamblysomus gunningi*, all at approximately 25% of dentary length (Fig. 8). We cannot rule out hyoid–dentary contact in *Namachloris*, but any such contact would probably have been less extensive than that seen in most extant chrysochlorids.Pickford (2015a: fig. 28) stated that in its postcranium, *Namachloris* exhibits a dorsally flat sternum (character 119), unlike extant chrysochlorids, in which the sternum is dorsally concave (Fig. 2C). The sternum otherwise resembles those of amblysomines and *Chlorotalpa* in having a triangular shape, with an elongated posterior process for articulation with the sternebrae. Pickford (2015a) also stated that *Namachloris* lacks a flexor canal in its distal radius (character 136), unlike any extant chrysochlorid species. The element described by Pickford (2015a: 181) as the clavicle of *Namachloris*, shaped like 'an old-fashioned barber's razor', is unlike any element we have observed in any extant chrysochlorid.

Our data place the Pleistocene fossil taxa *Chrysochloris arenosa* and *Chrysochloris bronneri* from Laangebaanweg (Asher and Avery 2010) within crown Chrysochloridae. Unexpectedly, our optimal parsimony topology (Fig. 12B) places *Chrysochloris arenosa* closer to *Eremitalpa* than *Chrysochloris*, contra Asher and Avery (2010), who regarded it as a species of *Chrysochloris*. In our Bayesian topologies derived from the combined dataset (Fig. 12A; Supporting Information, Fig. S1), *Chrysochloris arenosa* is unresolved. Until further data become available for these fossil species to better test this possibility, we do not propose to change their genus-level affiliations. Nonetheless, three characters support a closer affiliation of at least *Chrysochloris arenosa* with *Eremitalpa* than with *Chrysochloris asiatica*: reduction of the parastyle on P2 (character 84), a relatively narrow distal humeral margin (character 133) and a laterally oriented flexor process on the ventrum of digit III (character 148).

Among our fossil tenrecids, only two appear resolved in our non-clock analyses: *Erythrozootes* and *Parageogale* (Fig. 12). As previously suggested (Butler and Hopwood 1957, Butler 1984, Asher and Hofreiter 2006), *Parageogale* appears within the radiation of Malagasy tenrecids as sister taxon to *G. aurita*. Given its large amount of missing data (87%) and without temporal information (see below), Bayesian support for this clade is surprisingly high (pp = .98; Fig. 12A) and is based on several shared features: a reduced maxillary root of the zygoma (character 54), a large gap between its central upper incisors (character 78), an elongated infraorbital canal (character 58) and two premaxillary teeth (character 77). The last two features are also shared with *Erythrozootes*, which also appears within the Malagasy tenrec clade and comprises the sister taxon of a *Geogale–Parageogale* clade, albeit with weaker support (Fig. 12). *Erythrozootes* shares two further potential synapomorphies with *Geogale*: an unenlarged upper canine (character 80) and lack of an anteriorly projecting P3 parastyle (character 86).

Variation in the placement of the other tenrecid fossils in our sample is high. Even the strongly supported clade of extant potamogalines (Fig. 10, 11) becomes unresolved owing to the variable placement of these fossils (Fig. 12). Beyond the basic observation that *Arenagale*, *Nanogale*, *Promicrogale*, *Protenrec*

and *Sperrgale* are more likely to be related to extant tenrecids than to chrysochlorids, our dataset does not currently allow us to more precisely determine their affinities.

Timetree analysis

Applying broad uniform priors for the Eocliff fossils, which includes the Lutetian–Bartonian ages proposed for Eocliff by (respectively) Pickford *et al.* (2014: fig. 4) and Pickford (2015a), resulted in polytomies for many high-level clades, but not total-group Chrysochloridae (Supporting Information, Fig. S1). The latter formed a well-supported (pp = .99) clade, with slightly better resolution than the non-clock analysis of both extant and extinct taxa (Fig. 12A). *Namachloris* and *Prochrysochloris* composed the first two branches of total-group Chrysochloridae, with *Chrysochloris arenosa* and *Proamblysomus antiquus* in a polytomy alongside *Eremitalpa* and *Huetia* at the base of crown Chrysochloridae. Where resolved, the timetree reflected the same topology, with similar support levels, as our non-clock Bayesian analysis of extant taxa (Fig. 11A). Notably, and with the qualification that several key fossils are poorly resolved, the timetree shows a median age estimate for crown Chrysochloridae overlapping with that for the genus *Microgale* (Supporting Information, Fig. S1).

Although the resolution within Tenrecidae is poor, post-burn-in, tip age distributions for Eocliff fossils (Fig. 13) exhibit multiple but narrow peaks for *Arenagale calcareus*, *Sperrgale minutus* and *Namagale grandis*. These represent age estimates for different phylogenetic placements of each taxon, in particular as stem Tenrecinae, stem Potamogalinae or stem Tenrecidae. In contrast, there is a single peak for *Namachloris arenatans* at ~27 Myr (Fig. 13; Table 6), because its phylogenetic position as a stem chrysochlorid is uncontested.

All peaks of *Sperrgale minutus* and *Namagale grandis*, and the single peak of *Namachloris arenatans*, lie within the 20–30 Mya time window (Fig. 13), thereby suggesting a late Oligocene to earliest Miocene age for Eocliff. In contrast, the morphology of *Arenagale calcareus* allows different phylogenetic positions in different temporal windows at ~37, ~31 and ~22 Mya. Nevertheless, only one of its alternative phylogenetic placements suggests a pre-middle Oligocene age, whereas the other two are congruent with time estimates for *Sperrgale*, *Namagale* and *Namachloris*.

The tip age distribution of *Nanogale fragilis* also shows three narrow peaks, in accordance with its varying position as a stem tenrecid, stem chrysochlorid or placement outside of both clades. *Nanogale* is missing 93% of the characters in our matrix, and only *Promicrogale* (Pickford 2018) is worse, missing 95% (Table 4). There is a correspondingly weaker basis with which to apply a 'morphological clock' (Ronquist *et al.* 2012a) compared with more complete fossils, such as *Namachloris* (missing 32%). Nevertheless, all peaks for *Nanogale* are > 40 Mya, corresponding to an early Middle Eocene (Lutetian) minimum age for Black Crow, consistent with the temporal interpretation of Pickford *et al.* (2014) for this locality.

Re-running the analysis with narrow priors for Eocliff fossils (20–30 Mya, based on dates from the analysis with broad priors; see Fig. 13) increases resolution slightly. Branching patterns and support within chrysochlorids remain generally as before, except for a moderately supported clade uniting *Eremitalpa*, *Huetia* and *Chrysochloris arenosa* (pp = .75). The crown chrysochlorid node age is congruent using broad [mean = 16.48 Mya, 95% confidence interval (CI) = 13.40–19.67 Mya] and narrow (mean = 14.67 Mya, 95%CI = 12.56–18.31 Mya) priors for Eocliff fossils. Although there is a reasonably consistent signal placing the divergence of crown Chrysochloridae within the early to middle Miocene, the still uncertain placement of *Proamblysomus* has an effect. If it is within the crown, the date is correspondingly older (18–15 Mya); if it is on the stem, the date is younger (15–12 Mya). Either way, these results suggest a long ghost lineage, because *Proamblysomus* is known so far only from South African cave sites (Broom 1941, 1948b, Asher 2010, Mason *et al.* 2019), otherwise famous for their hominin primates and unlikely to pre-date the Pliocene (Reynolds and Kibii 2011).

Adding temporal data to our timetree analysis (Supporting Information, Fig. S1) weakens support for a *Geogale*–*Parageogale* clade. Using broad priors, the two appear in a clade in 54% of post-burn-in topologies; with narrow priors, this increases to 63%. However, owing to a temporal discrepancy among post-burn-in topologies, with most nodes showing contradictory, multi-modal age distributions, the timetree (Supporting Information, Fig. S1) does not resolve the temporal relationships between Tenrecini, Oryzorictini, *Geogale*, Potamogalinae and the fossils. Hence, and in contrast to the non-timetree analysis, *Geogale* and *Parageogale* are unresolved. The age of the *Microgale*–*Oryzorictes* split is approximately late Eocene (Table 6), and its divergence from the *Geogale* lineage is even older. Both events are much older than the age of *Parageogale* from the Miocene of Rusinga Island, Kenya (Butler and Hopwood 1957).

DISCUSSION AND CONCLUSIONS

Evolutionary tempo among insectivoran-grade afrotherians

Our analysis provides a basis to re-evaluate the ages of certain key fossil localities reported to yield chrysochlorid and tenrecid afrotherians. Eocliff in Namibia (Pickford *et al.* 2014, Pickford 2015a, b) is a particularly important site and has the most complete pre-Quaternary fossils of either group, whether its age is Lutetian (Pickford *et al.* 2014: fig. 4), Bartonian (Pickford 2015a) or younger (e.g., Sallam and Seiffert 2016, 2020). Eocliff fossils vary in terms of their temporal information content and amenability to the 'morphological clock' (Ronquist *et al.* 2012a), but the best-preserved (*Namachloris*) suggests that Eocliff is roughly between 22 and 30 Myr in age. This is similar to the interpretation of Sallam and Seiffert (2016, 2020) based on their analysis of rodents. The much more poorly preserved *Nanogale fragilis* (missing 93% of its morphological characters; see Table 4) is correspondingly less well resolved in our analysis, but to the extent that we recover any signal (Fig. 13; Supporting Information, Fig. S1), it is consistent with a Lutetian age proposed for Black Crow (Pickford *et al.* 2008, Mein and Pickford 2018).

Despite the lack of confidently resolved, pre-Pliocene crown fossils and some uncertainties about the high-level clades within the crown radiation, our results support an age of crown Chrysochloridae from the late Early to late Middle Miocene, regardless of the prior used for Eocliff fossils (Table 6).

Rooting extant golden moles

Analyses in which we excluded some or all tenrecids frequently supported a root node between a *Kilimatalpa–Chrysochloris–Cryptochloris* (Bayesian) or *Chrysochloris–Cryptochloris* (MP) clade and the remaining chrysochlorids. As shown in Table 7, using only *Procavia* and *Elephantulus* as outgroups yielded support for *Kilimatalpa–Chrysochloris–Cryptochloris* at the chrysochlorid root divergence, with Bayesian posterior probabilities ranging from .89 (BIC applied to DNA–indels) to .93 (AICc applied to DNA–indels–morphology). By adding *Echinops telfairi* Martin, 1838 and *Microgale talazaci*, these support values dropped to between .57 (BIC applied to DNA–indels) and .77 (AICc applied to DNA–indels–morphology). With all extant tenrecids included, the chrysochlorid root node flipped to the *Eremitalpa–Huetia* clade (BIC applied to DNA–indels; Fig. 10A) or became a polytomy [BIC applied to DNA–indels–morphology (Fig. 11A) and AICc applied to DNA–indels] or weakly supported the *Kilimatalpa–Chrysochloris–Cryptochloris* clade at the root position with a posterior probability of 0.56 (AICc applied to DNA–indels–morphology).

All but one of our equally weighted parsimony analyses of either DNA–indels or DNA–indels–morphology also supported a root placement for *Chrysochloris–Cryptochloris*, with the one exception being a polytomy owing to inclusion of all fossils (Table 7). Parsimony with equal weights reconstructed *Kilimatalpa* as the sister taxon to a *Huetia–Eremitalpa* clade. Applying implied weights and including all tenrecid species in our parsimony analyses changed the root position to *Eremitalpa* (Figs 10B, 11B, 12B; Table 7) and moved *Kilimatalpa* to the sister taxon of *Chrysochloris–Cryptochloris* (Figs 10B, 11B). This pattern reflects a correlation between larger samples of tenrecids, and departures from equally weighted parsimony, with ever weaker support for *Chrysochloris–Cryptochloris* and *Kilimatalpa* at the root position. This suggests that future studies with more data will favour a different root, most probably *Eremitalpa* and/or *Huetia* (Figs 10, 11, 12B).

The optimal parsimony topology, derived from an implied-weighting constant of $K = 4$, favoured *Eremitalpa* at the chrysochlorid root, with (Fig. 11B) or without (Fig. 10B) morphological data. Morphology changed the implied-weighting parsimony reconstruction of *Huetia*, moving it from the sister taxon of *Chlorotalpa* using only DNA–indels (Fig. 10B) to one node further crownward from the chrysochlorid root, after *Eremitalpa* (Fig. 11B). None of these placements exceeded 52% parsimony bootstrap support. Including fossils did not change the placement of *Huetia*, but as noted above in the non-timetree analysis (Fig. 12B), reconstructed the Pliocene fossil *Chrysochloris arenosa* adjacent to *Eremitalpa* at the base of crown Chrysochloridae.

Eremitalpa granti is a unique species within the Chrysochloridae (Fielden *et al.* 1990, Hickman 1990), a group which is itself derived relative to other mammals (MacPhee and Novacek 1993). However, in some respects *Eremitalpa* is plesiomorphic. For example, like *Huetia* (Fig. 6B), it lacks the distal hypertrophy of its stylohyoid bone (Fig. 6A) common in other chrysochlorids (Fig. 6C, D). Although it may exhibit hyoid–dentary contact, there is no clear articular facet on its stylohyoid for the angular process of the dentary (Fig. 6A), again similar to *Huetia* and anatomically consistent with their position outside the clade of other chrysochlorids (Figs 10A, 11, 12B). Furthermore, *Eremitalpa* is one of only a few species to lack interbullar trabeculation (Fig. 5; morphological character 8, state 1, also in *Chrysochloris asiatica*, *Cryptochloris*, *Chrysospalax* and *Carpitalpa*). Its ethmoid foramen opens into the temporal fossa anterior to the sphenorbital fissure (character 30, state 0), rather than directly into it as in other chrysochlorids. Its sphenorbital fissure is itself highly derived; in *Eremitalpa* it opens laterally (character 31, state 1) rather than anteriorly owing to displacement by the hypertrophied mallear head.

Some aspects of the dentition of *Eremitalpa* also differ from those of other chrysochlorids. For example, it lacks a parastyle on its second upper premolar (Fig. 7; character 84, state 1, also in *Chrysospalax*) and a lingual cusp on its third upper premolar (character 85, state 1, also in *Huetia*, *A. marleyi* and some specimens of *Calcochloris* and *A. corriae*). In its postcranial skeleton, *Eremitalpa* has a slightly less expanded distal margin of the humerus compared with humeral length. Along with *Chrysospalax*, *Hu. leucorhinus* and *A. corriae*, its distal width-to-length ratio is under .75 (character 133, state 1), in contrast to the ratio at or over .8 seen in other chrysochlorids (character 133, state 2). The distal phalanx of digital ray I in *Eremitalpa* is also relatively larger than those of other chrysochlorids and composes roughly three-quarters the length and width of the distal phalanx of digit II (Fig. 14; character 141, state 0), as opposed to the relatively smaller digit I distal phalanx of *A. hottentotus* (Fig. 14).

Cryptochloris wintoni exhibits the more typical chrysochlorid reduction of the digit I terminal phalanx, but both *Cryptochloris wintoni* and *Eremitalpa* possess the more plesiomorphic state of the first metacarpal being at least 80% as long as metacarpal II (Fig. 14; character 142, state 0). Other chrysochlorids exhibit a first-to-second metacarpal length ratio at or under .75 (character 142, state 1). *Cryptochloris wintoni* and *Eremitalpa* also uniquely exhibit a flexor process on the ventrum of the digit III terminal phalanx that extends laterally and not only ventrally (Fig. 14; character 148, state 1). *Eremitalpa* is unique in showing a bifid distal phalanx of digit IV that greatly exceeds the size of the distal phalanx of digit IV in other chrysochlorids (Fig. 14; character 149, state 1). It is also the only chrysochlorid to exhibit a species-typical thoracic vertebral count of 17 (character 152, state 4), with 38 of 42 individuals showing this number in the sample of Asher *et al.* (2011). Tenrecids such as *Setifer*, *Geogale* and *Potamogale* DuChaillu, 1861 also typically exhibit 17 thoracic vertebrae; some individuals of *Tenrec ecaudatus* Schreber, 1778 can exceed 20 (character 152, state 6). Other chrysochlorids range from 18–19 (e.g., *K. stuhlmanni*) to 19–20 thoracic vertebrae (e.g., *Neamblysomus gunningi*).

Eremitalpa shares with *Huetia* a relatively plesiomorphic hyoid apparatus (Fig. 6). Both taxa may show some hyoid–dentary contact, but neither has a clear articular facet on the stylohyoid for the lower jaw (character 69). The stylohyoid of *Eremitalpa* shows only a slight angle between its proximal and distal components (character 70; see Fig. 6A), similar to some other chrysochlorids (e.g., *Cryptochloris wintoni*; Fig. 6D), but in contrast to the sharper division evident between proximal and distal ends of the stylohyoid seen among amblysomines (character 70; Fig. 6C). As in tenrecids and *Huetia*, *Eremitalpa* lacks

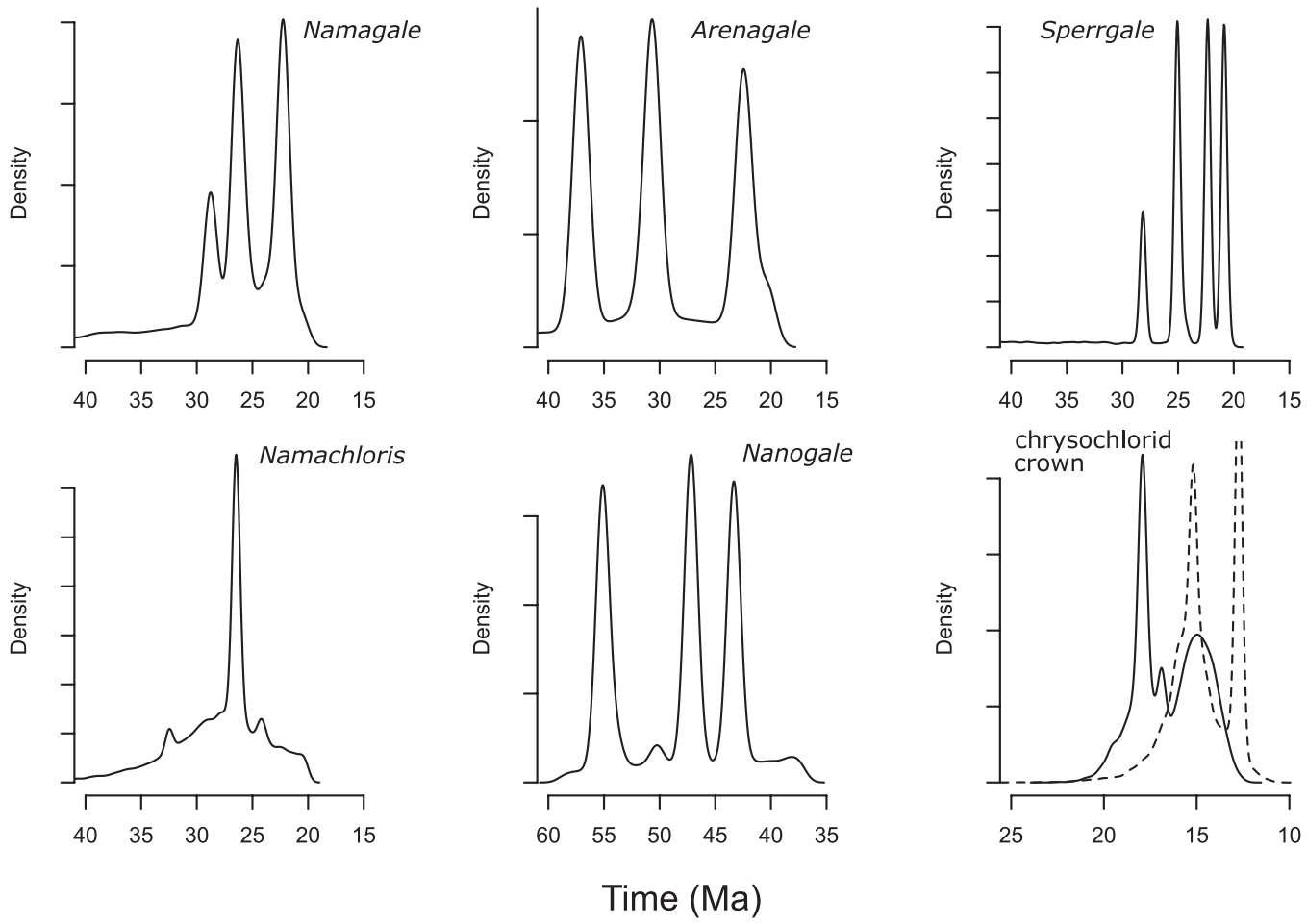

Figure 13. Age distributions for fossil tip taxa from Eocliff (*Namagale*, *Arenagale*, *Sperrgale* and *Namachloris*), Black Crow (*Nanogale*) and crown Chrysochloridae. Continuous and dashed lines indicate analyses with (respectively) broad and narrow fossil priors (see Materials and methods).

a pronounced bulbous expansion of its distal stylohyoid (character 71; Fig. 6A). In *Huetia*, there is no angle but only a slight curve between proximal and distal ends (Fig. 6B). The anteroposterior length of the angular process of the dentary shows some correspondence to the extent of the articular facet on the stylohyoid. Among extant chrysochlorids, the angular process is shortest in *Huetia* (character 68; Fig. 6B), followed closely by *Eremitalpa* (Fig. 6A), both under 15% of dentary length. As noted above, it may reach approximately 25% of jaw length in species of *Amblysomus* (Fig. 6C) and *Chrysochloris asiatica*.

Furthermore, *Eremitalpa* exhibits the smallest diploid chromosome number of any chrysochlorid, with one female figured by Gilbert *et al.* (2006: fig. 2d) showing $2n = 26$ (character 173, state 0). As noted above, most other chrysochlorids have $2n = 30$; *A. robustus* and *A. septentrionalis* have, respectively, 36 and 34. *Calcochloris obtusirostris* has 28 (Bronner 1995b, Gilbert *et al.* 2006, 2008). The only other taxon in our sample with a diploid chromosome number of 26 is the macroscelidid, *Elephantulus* (Smit *et al.* 2011). The tenrecid *G. aurita* has even fewer chromosomes, with $2n = 14$ (Gilbert 2008).

Our results do not resolve the phylogenetic affinities of *Huetia* decisively, but we can rule out genus-level affiliations with *Amblysomus* (Simonetta 1968), *Chlorotalpa* (Meester 1974) and *Calcochloris* (Bronner 1995a, b). Furthermore, *Huetia* has the most plesiomorphic hyoid apparatus of any extant chrysochlorid, along with an angular process of the dentary that resembles the one illustrated for *Namachloris* (Pickford 2015a: figs 12, 19). Anatomically, and as noted above, some specimens of *Hu. leucorhinus* share with amblysomines middle-ear features related to a relatively unexpanded malleus. *Huetia* also shares with *Eremitalpa* a distal width-to-length ratio of the humerus below .75 (character 133).

Among our more unprecedented results for chrysochlorids is the monophyly of *Calcochloris obtusirostris* with *Chrysospalax*, showing posterior probabilities of 1.0 (Figs 10, 11) or .98 (Supporting Information, Fig. S1), but dropping to .79 in the non-timetree analysis including fossils (Fig. 12). No previous anatomical (e.g., Simonetta 1968, Petter 1981, Bronner 1995a) or cytogenetic (e.g., Gilbert *et al.* 2008) study of golden moles suggested this relationship, although it did appear weakly supported in an analysis of growth hormone receptor sequences alone (*GHR* exon 10; see Asher *et al.* 2010: fig. 4). With the qualification that support for this clade drops with the inclusion of fossils (Fig. 12), a result which reflects ambiguity in the placement of fossils rather than living species, we regard this surprising relationship as valid and worthy of a high-level taxon, which we here dub Chrysospalacinae (Figs 10, 11).

Table 6. Median and 95% confidence intervals (CI) of afrotherian, tenrecid and chrysochlorid node ages (in millions of years) from the consensus timetree (Supporting Information, Fig. S1) based on the analysis using broad priors for Eocliff fossils. For abbreviations and definitions of high-level clades, see Figure 10.

Crown node	Plus fossils?	Median	Lower 95% CI	Upper 95% CI
Afrotheria		67.21	61.16	77.98
Procavia + Macroscelididae		55.33	43.4	66.21
Tenrecidae	*Nanogale*	63.26	56.81	66.39
Potamogalinae (Po)		37.55	36.42	39.79
Oryzorictini (Oi)		34.43	28.93	38.11
Tenrecini (Ti)		29.29	26.05	32.93
Tenrecina (Ta)		20.39	19.66	22.22
Microgale		17.3	13.76	20.36
Microgale cowani + *Mi. longicaudataus* + *Mi. mergulus*		13.47	11.52	17.16
Microgale longicaudatus + *Mi. mergulus*		11.55	9.98	14.86
Setiferina (Sa)		9.75	9.36	14.86
Microgale dobsoni + *Mi. talazaci*		7.07	4.43	7.39
Chrysochloridae	*Namachloris* + *Prochryochloris* + *Proamblysomus*	34.66	26.21	42.79
Chrysochloridae	*Prochryochloris* + *Proamblysomus*	27.3	20.84	34.96
Chrysochloridae	*Proamblysomus*	17.97	12.97	29.14
Chrysochlorinae	*Chrysochloris bronneri*	11.55	10.13	14.45
Amblysominae + *Chlorotalpa* + Chryso spalacinae		10.99	9.16	14.1
Amblysominae + *Chlorotalpa*		9.21	7.78	14
Amblysominae (Am)		9.12	6.57	10.11
Chrysospalacinae (Cx)		7.67	7.57	12.25
Chrysochloris asiatica + *Cryptochloris*	*Chrysochloris bronneri*	7.43	6.17	10.26
Carpitalpa + *Neamblysomus*		6.69	5.19	8.36
Amblysomus		3.53	2.74	5.87
Chrysochloris asiatica + *Cryptochloris*		3.46	2.06	3.68
Chrysospalax		3.45	2.16	4.07
Amblysomus corriae + *A. hottentotus* + *A. robustus* + *A. septentrionalis*		2.2	1.53	3.04
Neamblysomus		2.05	1.56	2.63
Amblysomus hottentotus + *A. robustus* + *A. septentrionalis*		1.68	0.96	2.07
Amblysomus marleyi + *A. meesteri*		1.64	1.08	2.62
Chlorotalpa		0.9	0.37	1.9
Amblysomus robustus + *A. septentrionalis*		0.71	0.23	0.84
Cryptochloris		0.69	0.17	1

Variation in tropical chrysochlorids

Two golden mole species have wide distributions outside southern Africa: *Kilimatalpa stuhlmanni* and *Huetia leucorhinus*. Both exhibit intraspecific variation. Two CT-scanned *Kilimatalpa* specimens in our sample are from areas in which only this species is known (Bronner 1995a: fig. 1.1): ZMB-Mam 76775 from 'Ussagara, Nguru' (Tanzania) and AMNH 82372 from well over 1000 km to the west, in 'North Kivu' [north-east Democratic Republic of the Congo (DRC)]. The AMNH specimen shows the elongated malleus (cf. Bronner 1995a: fig. 9.1) and temporal bulla typical for this species. The ZMB specimen also shows an enlarged mallear head but is not as elongated. Without further data from tropical African chrysochlorid populations, we propose neither a range extension nor a new species to accommodate this variation, both of which would require further phylogeographical study.

To code morphological characters of *Hu. leucorhinus*, we sampled CT scans of one alcohol-preserved cadaver (AMNH 118829 from 'Kinkala', DRC), three macerated skulls (MNHN CG1901–CG1083 from 'Haute-Sangha', Congo, BMNH (also known as NHMUK) 26.7.6.154 from Luluabourg, DRC, BMNH 63.1012 from 'Nordeste, Poste de Canzar', Angola) and a disarticulated skeleton (FMNH 81734 from Cuanza Norte, Angola). We also examined a CT scan of a skin containing

Table 7. Chrysochlorid root positions depending on optimality criterion, model selection criteria, inclusion of morphological data, tenrecids and fossils. The column 'Optimality' shows results using equally weighted parsimony (eq), implied weighting with concavity constants of two (*K*2) and four (*K*4). The column 'Tenrecs' refers to the number of excluded tenrecs, either all (excluded) or all but *Echinops* and *Microgale talazaci* (Echinops-Mtal). 'Root pp' refers to the posterior probability of the first branching event within crown Chrysochloridae (if resolved and applicable only to Bayesian analyses). Asia = *Chrysochloris asiatica*, crypto = *Cryptochloris*, Eremi = *Eremitalpa*, Kili = *Kilimatalpa*, MPTs = Most Parsimonious Trees.

Name	Optimality	Morph	Tenrecs	Fossils	MPTs	Length	Root	Root pp
extant	eq	Included	Included	Excluded	2	10054	*Asia-crypto*	
extant*K*2	*K*2	Included	Included	Excluded	1	978.35	*Eremi*	
extant*K*4	*K*4	Included	Included	Excluded	1	702.15	*Eremi* then *Huetia*	
dna	eq	Excluded	Included	Excluded	2	9551	*Asia-crypto*	
dna*K*2	*K*2	Excluded	Included	Excluded	1	922.01	*Eremi*	
dna*K*4	*K*4	Excluded	Included	Excluded	1	662.83	*Eremi*	
all	eq	Included	Included	Included	2772	10098	Polytomy	
all*K*2	*K*2	Included	Included	Included	485	982.81	*Eremi* + *arenosa*	
all*K*4	*K*4	Included	Included	Included	72	705.94	*Eremi* + *arenosa* then *Huetia*	
dnaEcTa	eq	Excluded	Echinops-Mtal	Excluded	2	5841	*Asia-crypto*	
dna*K*2EcTa	*K*2	Excluded	Echinops-Mtal	Excluded	1	534.88	*Asia-crypto*	
dna*K*4EcTa	*K*4	Excluded	Echinops-Mtal	Excluded	1	363.5	*Asia-crypto*	
extantNT	eq	Included	Excluded	Excluded	1	4839	*Asia-crypto*	
extant*K*2NT	*K*2	Included	Excluded	Excluded	1	417.34	*Asia-crypto*	
extant*K*4NT	*K*4	Included	Excluded	Excluded	1	283.1	*Asia-crypto*	
extantEcTa	eq	Included	Echinops-Mtal	Excluded	2	6201	*Asia-crypto*	
extant*K*2EcTa	*K*2	Included	Echinops-Mtal	Excluded	1	570.75	*Asia-crypto*	
extant*K*4EcTa	*K*4	Included	Echinops-Mtal	Excluded	1	387.92	*Asia-crypto*	
dnaNT	eq	Excluded	Excluded	Excluded	1	4541	*Asia-crypto*	
dna*K*2NT	*K*2	Excluded	Excluded	Excluded	1	392.43	*Asia-crypto*	
dna*K*4NT	*K*4	Excluded	Excluded	Excluded	1	265.64	*Asia-crypto*	
all12febAIC	Bayes-AICc	Included	Included	Included			Polytomy	
dna12febAIC	Bayes-AICc	Excluded	Included	Excluded			Polytomy	
dna12febAICEcTa	Bayes-AICc	Excluded	Echinops-Mtal	Excluded			*Kili-chryso-crypto*	0.76
dna12febAICNoTrec	Bayes-AICc	Excluded	Excluded	Excluded			*Kili-chryso-crypto*	0.93
ext12febAIC	Bayes-AICc	Included	Included	Excluded			*Kili-chryso-crypto*	0.56
ext12febAICEcTa	Bayes-AICc	Included	Echinops-Mtal	Excluded			*Kili-chryso-crypto*	0.77
ext12febAICNoTrec	Bayes-AICc	Included	Excluded	Excluded			*Kili-chryso-crypto*	0.93
all19dec	Bayes-BIC	Included	Included	Included			Polytomy	
dna19dec	Bayes-BIC	Excluded	Included	Excluded			*Eremi-Huetia*	0.59
dna19decEcTa	Bayes-BIC	Excluded	Echinops-Mtal	Excluded			*Kili-chryso-crypto*	0.57
dna19decNoTrec	Bayes-BIC	Excluded	Excluded	Excluded			*Kili-chryso-crypto*	0.89
ext19dec	Bayes-BIC	Included	Included	Excluded			Polytomy	
ext19decEcTa	Bayes-BIC	Included	Echinops-mtal	Excluded			*Kili-chryso-crypto*	0.73
ext19decNoTrec	Bayes-BIC	Included	Excluded	Excluded			*Kili-chryso-crypto*	0.9
timetree	Bayes-BIC	Included	Included	Included			Polytomy	

rostral fragments and distal limb elements (NHMW B2742 from Stanley Falls, DRC). 'Sangha' is a province in northern Congo, nearly 2000 km north of Cuanza Norte, Angola and 1300 km west of Luluabourg, DRC. This comprises an area greater than the whole of South Africa, and it should come as no surprise that populations of small, fossorial mammals separated by such distances show variation.

Our sample of *Huetia* shows eight anatomical polymorphisms, more than any other species. Using some of the same CT scans, we confirm the ossicular polymorphisms observed by Mason *et al.* (2017), in particular that specimens of *Huetia* from Congo and the DRC show a more expanded mallear head (character 14) than specimens from Angola. We also observed a slightly more concave facet on the malleus in BMNH 26.7.6.154 (Luluabourg, DRC) than in other specimens (character 16). Chrysochlorids generally lack an alisphenoid canal (character 32), as do most specimens of *Huetia*. However, we observed on AMNH 118829 a bridge of bone on either side, covering a depression anterior to the foramen ovale leading towards the sphenorbital fissure, corresponding to an alisphenoid canal. The posterolateral palate, ventral to the sphenopalatine foramen, in the two BMNH specimens is relatively flat and lacks

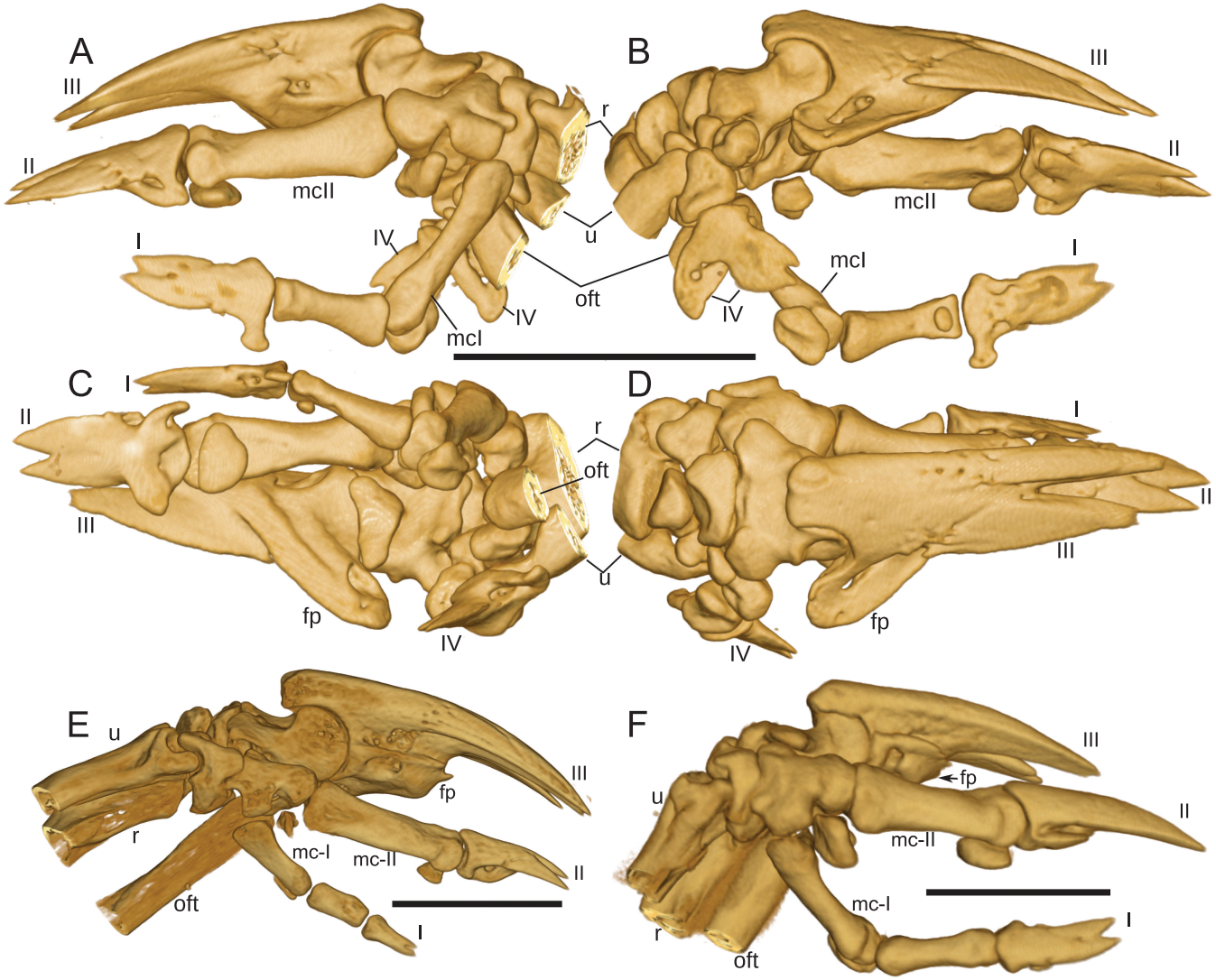

Figure 14. Right hand skeleton of *Eremitalpa granti* (NRM-MA 641288) in medial (A), lateral (B), ventral (C) and dorsal (D) views. Medial views of left hand skeletons of *Amblysomus hottentotus* (E; MCZ 57045) and *Cryptochloris wintoni* (F; NRM-MA 641436). Roman numerals indicate digital rays. Abbreviations: fp, flexor process; mc, metacarpal; oft, ossified flexor tendon; r, radius; u, ulna. Scale bars (one for A–D; one each for E, F): 5 mm.

a clear indication of a common recess for the sphenopalatine and dorsal palatine foramina (character 48). This area is more rugose in MNHN CG1901-1083 (Sangha, Congo), suggestive of separate dorsal and sphenopalatine foramina. The ratio of palatal width to postpalatal length (character 64) and skull length to width (character 66) are also polymorphic in *Huetia*. Protocones on the M1 (character 90) of most specimens are lacking; in AMNH 118829 (Kinkala, DRC) they are small but evident on the cingulum. Among our postcranial characters, *Huetia* is polymorphic for only one: depth of the sesamoid groove on the posterior aspect of the distal tibia (character 167). FMNH 81734 (from Angola) exhibits such a groove, whereas NHMW B2742 (Stanley Falls, DRC) and AMNH 118829 (Kinkala, DRC) do not. These were the only CT-scanned specimens with postcrania available to us; considering further specimens would likely increase the number of polymorphisms. Our sample of molecular data from *Huetia* derives from Maree S, Bronner GN, Bennett NC, Oosthuizen CJ, Asher RJ, Hofreiter M, Bloomer P (2014, unpublished work; see Supporting Information, Appendix S1), who reported a single source: a specimen 'found by student in a Kinshasa garden, but lost before deposition as voucher'. This specimen yielded sequences for four of our six loci (12S rRNA, *cytB*, *GHR* and *stat5a*), but not the other two (*vWF* and *ND2*).

Given the anatomical variation among specimens of *Huetia* and *Kilimatalpa* across their large ranges, we recommend that future studies consider a more fine-grained sampling regimen, perhaps comparable to the study of *Amblysomus* by Mynhardt *et al.* (2015). Such an analysis would better resolve the variation we have observed, which might even subsume the long-enigmatic '*Calcochloris tytonis*', not sampled in this study and known from a single specimen preserved in an owl pellet from Somalia (Simonetta 1968). None of our analyses places *Huetia* by itself as sister to all other extant chrysochlorids (Figs 10–12; Table 7), but an affinity for *Eremitalpa*, together with which it might form the sister clade to other crown species, forms a key hypothesis for future studies to test.

Frustratingly, *Huetia* is one of a small number of chrysochlorid species for which we lack data on chromosomal morphology. We also lack sequences for two of our loci from this taxon: *vWF* and *ND2* (Table 1). If *Huetia* is the sister taxon of *Eremitalpa*, as weakly suggested in our optimal Bayesian results (Figs 10A, 11A), we would expect the chromosome number of *Huetia* to resemble that of *Eremitalpa* (where $2n = 26$), not the more common $2n = 30$ shown by most other chrysochlorid species (Bronner 1995a). In contrast, if *Huetia* shows a more typically chrysochlorid karyotype of $2n = 30$, this would be consistent with the topology favoured by our optimal, implied-weighting parsimony result based on DNA–indels (Fig. 10B), in which *Eremitalpa* alone comprises the sister taxon to all other extant chrysochlorids, and *Huetia* is the sister taxon of *Chlorotalpa*.

Based partly on the relatively plesiomorphic anatomy of its hyoid apparatus and angular process of the dentary, we regard the latter possibility as unlikely. As currently defined, *Hu. leucorhinus* has one of the largest ranges of any extant chrysochlorid and is separated from most other species by hundreds or thousands of kilometres. Our results suggest that uncovering the phenotypic and molecular diversity of tropical species, *Huetia* in particular, should be a goal for future studies, one which promises to further resolve the evolutionary history of insectivoran-grade Afrotheria.

SUPPLEMENTARY DATA

Supplementary data are available at *Zoological Journal of the Linnean Society* online.

Appendix S1. Provides methods for collecting molecular data.

Appendix S2. Provides the DNA alignments, indel and morphological characters.

Figure S1. Depicts the timetree.

Our morphological dataset is graphically documented and available via our morphobank project page: http://morphobank.org/permalink/?P4214.

ACKNOWLEDGEMENTS

We thank all the curators and collections staff at museums who, over the course of many years, hosted our visits and helped to enable data collection on extant and fossil mammals. G.N.B. and R.J.A. thank Denise Hamerton, Margaret Avery, Deano Stynder and Kermit van Willingh at the Iziko South African Museum in Cape Town; Teresa Kearney, Stephanie Potze and Francis Thackeray at the Ditsong (formerly Transvaal) Museum in Pretoria; Lloyd Wingate, Fred Kigozi and Lucas Thibedi at the Amathole Museum in King Williams Town; and Emma Mbua at the National Museums of Kenya. S.M. thanks Jofred Opperman at the Iziko South African Museum in Cape Town. R.J.A. thanks the University of Cambridge Department of Zoology, the Royal Society and the Leverhulme Trust for financial support. N.C.B. thanks a DST-NRF South African Research Chair for Mammalian Behavioural Ecology and Physiology (GUN 64756). S.M. thanks Nigel Bennett and the National Research Foundation (NRF) for grantholder-linked postdoctoral fellowship support (2022). R.J.A. and S.M. thank Carlyn Wells at the Stellenbosch University Central Analytical Facilities (CAF) for assistance with CT scans. All authors thank Nigel Bennett for 20 years of support for fieldwork to broaden our understanding of golden moles. R.J.A. thanks Susy Cote and Erik Seiffert for discussion and access to a CT scan of *Erythrozootes*; Matt Mason and Martin Pickford for access to CT scans of *Namachloris arenatans* and *Proamblysomus antiquus*; and Matt Mason for access to CT scans of NHM-London specimens of *Huetia leucorhinus* and *Calcochloris obtusirostris*. For access to other CT scans, we thank Robert Voss, Marisa Surovy, and Neil Duncan at the American Museum of Natural History; April Neander and ZheXi Luo at the University of Chicago; Lawrence Heaney and Adam Ferguson at the Field Museum of Natural History; Daniela Kalthoff at the Naturhistoriska Riksmuseet Stockholm; Tunhe Zhao at the Stockholm University Brain Imaging Centre; Mark Omura, Greg Lin and Jim Reynolds at the Harvard Museum of Comparative Zoology; Cody Thompson at the University of Michigan Museum of Zoology; Roberto Portela Miguez and Vincent Fernandez at the Natural History Museum London; Ket Smithson, Matt Lowe and Natalie Jones at the University Museum of Zoology Cambridge; Carol Spencer at the Museum of Vertebrate Zoology at the University of California Berkeley; Nikolay Kardjilov at the Helmholtz-Zentrum Berlin; and Arriana Harrington, Justin Gladman and Doug Boyer at Duke University. For information on the provenance of *Amblysomus* sequences derived from specimen T1903, R.J.A. thanks Mark Springer and Carey Krajewsji. We are also grateful to Franco Basso for advice on Latin grammar and to Matt Mason, two anonymous reviewers and the Editors for constructive critiques of the text. All the authors thank Paulette Bloomer, Sarita Maree and Carel Oosthuizen for their help in generating data and with early versions of this manuscript.

AUTHOR CONTRIBUTIONS

Gary N. Bronner conceived the project and organized and undertook relevant fieldwork to obtain major parts of our dataset. Samantha Mynhardt contributed molecular data and obtained CT scans of several specimens. Nigel C. Bennett helped to conceive the project, organized fieldwork, obtained funding and key specimens, and contributed data. Lientjie Cohen facilitated fieldwork and data collection. Michael Hofreiter and Nick Crumpton contributed data. Patrick Arnold undertook the timetree analysis and wrote that part of the draft. Robert J. Asher undertook the other analyses, obtained CT scans, participated in fieldwork, collected morphological data and wrote the initial drafts of the manuscript. All authors helped with the analyses, and read and contributed to the final version of the manuscript.

CONFLICT OF INTEREST

The authors declare no conflicts of interest.

DATA AVAILABILITY

The data underlying this article are available in the article and in its online supplementary material.

REFERENCES

Álvarez-Carretero S, Tamuri AU, Battini M *et al.* A species-level timeline of mammal evolution integrating phylogenomic data. *Nature* 2022;**602**:263–7.

Asher RJ. Tenrecoidea. In: Werdelin L, Sanders WJ (eds), *Cenozoic Mammals of Africa*. Berkeley: University of California Press, 2010, 99–106.

Asher RJ. Recent additions to the fossil record of tenrecs and golden moles. *Afrotherian Conservation* 2019;**15**:4–13.

Asher RJ, Avery DM. New golden moles (Afrotheria, Chrysochloridae) from the Pliocene of South Africa. *Paleontologica Electronica* 2010;**13**:3A.

Asher RJ, Helgen KM. Nomenclature and placental mammal phylogeny. *BMC Evolutionary Biology* 2010;**10**:102.

Asher RJ, Hofreiter M. Tenrec phylogeny and the noninvasive extraction of nuclear DNA. *Systematic Biology* 2006;**55**:181–94.
Asher RJ, Lin KH, Kardjilov N, *et al*. Variability and constraint in the mammalian vertebral column. *Journal of Evolutionary Biology* 2011;**24**:1080–90.
Asher RJ, Maree S, Bronner GN *et al*. A phylogenetic estimate for golden moles (Mammalia, Afrotheria, Chrysochloridae). *BMC Evolutionary Biology* 2010;**10**:69.
Asher RJ, Sánchez-Villagra MR. Locking yourself out: diversity among dentally zalambdodont therian mammals. *Journal of Mammalian Evolution* 2005;**12**:265–82.
Asher RJ, Seiffert ER. Afrotheria. In: Werdelin L, Sanders WJ (eds), *Cenozoic Mammals of Africa*. Berkeley: University of California Press, 2010, 911–28.
Bapst DW. paleotree: an R package for paleontological and phylogenetic analyses of evolution. *Methods in Ecology and Evolution* 2012;**3**:803–7.
Bhagwandin A, Ndlovu N, Bronner GN *et al*. The hypercholinergic brain of the Cape golden mole (*Chrysochloris asiatica*). *Journal of Chemical Neuroanatomy* 2020;**110**:101856.
Borgaonkar DS, Gould E. Homozygous reciprocal translocation as a mode of speciation in *Microgale* Thomas 1883 (Tenrecidae-Insectivora). *Experientia* 1968;**24**:506–9.
Bronner GN. Comparative hyoid morphology of nine chrysochlorid species (Mammalia: Chrysochloridae). *Annals of the Transvaal Museum* 1991;**35**:295–311.
Bronner GN. *Systematic revision of the golden mole genera: Amblysomus, Chlorotalpa and Calcochloris (Insectivora: Chrysochloromorpha; Chrysochloridae)*. PhD Thesis, Durban: University of Natal, 1995a.
Bronner GN. Cytogenetic properties of nine species of golden moles (Insectivora: Chrysochloridae). *Journal of Mammalogy* 1995b;**76**:957–71.
Bronner GN. New species and subspecies of golden mole (Chrysochloridae: Amblysomus) from Mpumalanga, South Africa. *Mammalia* 2000;**64**:41–54.
Bronner GN, Bennett NC. Family Chrysochloridae. In Skinner JD, Chimimba CT (eds), *The Mammals of the Southern African Sub-Region*. Cambridge: Cambridge University Press, 2005.
Bronner GN, Jenkins PD. Order Afrosoricida. In: Wilson DE, Reeder DM (ed.), *Mammal Species of the World: a Taxonomic and Geographic Reference*. Baltimore: Johns Hopkins University Press, 2005, 71–81.
Bronner GN, Jones E, Coetzer DJ. Hyoid-dentary articulations in golden moles (Mammalia: Insectivora; Chrysochloridae). *Zeitschrift für Säugetierkunde* 1990;**55**:11–5.
Broom R. On two Pleistocene golden moles. *Annals of the Transvaal Museum* 1941;**20**:215–6.
Broom R. Some further advances in our knowledge of the Cape golden moles. *Annals of the Transvaal Museum* 1948a;**21**:234–41.
Broom R. Some South African Pliocene and Pleistocene mammals. *Annals of the Transvaal Museum* 1948b;**21**:1–38.
Butler PM. Studies of the mammalian dentition.–I. The teeth of *Centetes ecaudatus* and its allies. *Proceedings of the Zoological Society of London* 1937;**B107**:103–32.
Butler PM. Insectivora and Chiroptera. In: Maglio VJ, Cooke HBS (eds), *Evolution of African Mammals*. Cambridge: Harvard University Press, 1978, 56–68.
Butler PM. Macroscelidea, Insectivora and Chiroptera from the Miocene of east Africa. *Palaeovertebrata* 1984;**14**:117–98.
Butler PM, Hopwood AT. Insectivora and Chiroptera from the Miocene rocks of Kenya Colony. *British Museum Fossil Mammals of Africa* 1957;**13**:1–35.
Coster P, Benammi M, Mahboubi M *et al*. Chronology of the Eocene continental deposits of Africa: magnetostratigraphy and biostratigraphy of the El Kohol and Glib Zegdou Formations, Algeria. *GSA Bulletin* 2012;**124**:1590–606.
Crumpton N, Kardjilov N, Asher RJ. Convergence vs. specialization in the ear region of moles (Mammalia). *Journal of Morphology* 2015;**276**:900–14.
De Graaff G. A new chrysochlorid from Makapansgat. *Palaeontologia Africana* 1958;**5**:21–7.
Everson KM, Soarimalala V, Goodman SM *et al*. Multiple loci and complete taxonomic sampling resolve the phylogeny and biogeographic history of tenrecs (Mammalia: Tenrecidae) and reveal higher speciation rates in Madagascar's humid forests. *Systematic Biology* 2016;**65**:890–909.
Faurby S, Svenning JC. A species-level phylogeny of all extant and late Quaternary extinct mammals using a novel heuristic-hierarchical Bayesian approach. *Molecular Phylogenetics and Evolution* 2015;**84**:14–26.
Fielden LJ, Perrin MR, Hickman GC. Feeding ecology and foraging behaviour of the Namib Desert golden mole, *Eremitalpa granti namibensis* (Chrysochloridae). *Journal of Zoology* 1990;**220**:367–89.
Forcart L. Beiträge zur Kenntnis der Insectivoren Familie Chrysochloridae. *Revue Suisse de Zoologie* 1942;**49**:1–6.
Forster-Cooper C. On the ear region of certain of the Chrysochloridae. *Philosophical Transactions of the Royal Society of London, Series B* 1928;**216**:265–83.
Gilbert C. *Chromosomal evolution and phylogeny of golden moles and tenrecs (Mammalia: Afrosoricida)*. PhD Thesis, Stellenbosch: University of Stellenbosch, 2008.
Gilbert C, Goodman SM, Soarimalala V *et al*. Chromosomal evolution in tenrecs (*Microgale* and *Oryzorictes*, Tenrecidae) from the Central Highlands of Madagascar. *Chromosome Research* 2007;**15**:1075–91.
Gilbert C, Maree S, Robinson TJ. Chromosomal evolution and distribution of telomeric repeats in golden moles (Chrysochloridae, Mammalia). *Cytogenetic and Genome Research* 2008;**121**:110–9.
Gilbert C, O'Brien PC, Bronner GN *et al*. Chromosome painting and molecular dating indicate a low rate of chromosomal evolution in golden moles (Mammalia, Chrysochloridae). *Chromosome Research* 2006;**14**:793–803.
Goloboff PA. Estimating character weights during tree search. *Cladistics* 1993;**9**:83–91.
Goloboff PA, Carpenter JM, Arias JS *et al*. Weighting against homoplasy improves phylogenetic analysis of morphological data sets. *Cladistics* 2008;**24**:758–73.
Goloboff PA, Catalano SA. TNT version 1.5, including a full implementation of phylogenetic morphometrics. *Cladistics* 2016;**32**:221–38.
Gunnell GF, Boyer DM, Friscia AR *et al*. Fossil lemurs from Egypt and Kenya suggest an African origin for Madagascar's aye-aye. *Nature Communications* 2018;**9**:3193.
Hickman GC. The Chrysochloridae: studies toward a broader perspective of adaptation in subterranean mammals. *Progress in Clinical and Biological Research* 1990;**335**:23–48.
Hu Y, Limaye A, Lu J. Three-dimensional segmentation of computed tomography data using Drishti Paint: new tools and developments. *Royal Society Open Science* 2020;**7**:201033.
Huet M. Note sur une espece nouvelle de Chrysochlore de la cöte du golfe de Guinee. *Nouvelles Archives du Muséum d'Histoire Naturelle* 1885;**2**:1–16.
Lanfear R, Calcott B, Ho SYW *et al*. PartitionFinder: combined selection of partitioning schemes and substitution models for phylogenetic analyses. *Molecular Biology and Evolution* 2012;**29**:1695–701.
Lanfear R, Frandsen PB, Wright AM *et al*. PartitionFinder 2: new methods for selecting partitioned models of evolution for molecular and morphological phylogenetic analyses. *Molecular Biology and Evolution* 2016;**34**:772–3.
Langer P. *Comparative Anatomy of the Gastrointestinal Tract in Eutheria I: Taxonomy, Biogeography and Food: Afrotheria, Xenarthra and Euarchontoglires*. Berlin: Walter de Gruyter, 2017.
Limaye A. Drishti-volume exploration and presentation tool. *Spie Digital Library* 2012:85060X. https://doi.org/10.1117/12.935640
Lundholm BG. Descriptions of new mammals. *Annals of the Transvaal Museum* 1954;**22**:279–303.
MacPhee RDE, Novacek MJ. Definition and relationships of Lipotyphla. In: Szalay FS, Novacek MJ, Mckenna MC (eds), *Mammal Phylogeny, Vol. 2: Placentals*. New York: Springer, 1993, 13–31.
Maddison WP, Maddison DR. 2019. Mesquite: a modular system for evolutionary analysis. *Version 3.81*. http://www.mesquiteproject.org

Madeira F, Pearce M, Tivey ARN *et al*. Search and sequence analysis tools services from EMBL-EBI in 2022. *Nucleic Acids Research* 2022;**50**:W276–9.
Marivaux L, Essid EM, Marzougui W *et al*. A new and primitive species of *Protophiomys* (Rodentia, Hystricognathi) from the late middle Eocene of Djebel el Kébar, Central Tunisia. *Palaeovertebrata* 2014;**38**:e2.
Mason MJ. Morphology of the middle ear of golden moles (Chrysochloridae). *Journal of Zoology* 2003;**260**:391–403.
Mason MJ. Functional morphology of the middle ear in *Chlorotalpa* golden moles (Mammalia, Chrysochloridae): predictions from three models. *Journal of Morphology* 2004;**261**:162–74.
Mason MJ, Bennett NC, Pickford M. The middle and inner ears of the Palaeogene golden mole *Namachloris*: a comparison with extant species. *Journal of Morphology* 2017;**279**:375–95.
Mason MJ, Bennett NC, Pickford M. A fossil chrysochlorid skull in the Ditsong National Museum of Natural History: Robert Broom's missing specimen unearthed? *Palaeontologia Africana* 2019;**53**:207–18.
Meester JAJ. Family Chrysochloridae. In: Meester JAJ, Setzer HW (eds), *The Mammals of Africa: an Identification Manual*. Washington: Smithsonian Institution Press, 1974, 1–7.
Mein P, Pickford M. Insectivora from Arrisdrift, a basal Middle Miocene locality in southern Namibia. *Memoir of the Geological Survey of Namibia* 2003;**19**:143–6.
Mein P, Pickford M. Early Miocene Insectivores from the Northern Sperrgebiet, Namibia. *Memoir of the Geological Survey of Namibia* 2008;**20**:169–84.
Mein P, Pickford M. Reithroparamyine rodent from the Eocene of Namibia. *Communications of the Geological Survey of Namibia* 2018;**18**:38–47.
Mynhardt S, Maree S, Pelser I *et al*. Phylogeography of a morphologically cryptic golden mole assemblage from South-Eastern Africa. *PLoS One* 2015;**10**:e0144995.
Olson LE, Goodman SM. Phylogeny of Madagascar's tenrecs (Lipotyphla, Tenrecidae). In: Goodman SM, Benstead JP (eds), *Natural History of Madagascar*. Chicago: University of Chicago Press, 2003, 1235–42.
Pardini AT. *Genome evolution and systematics of the Paenungulata (Afrotheria, Mammalia)*. PhD Thesis, Stellenbosch: University of Stellenbosch, 2006.
Pardini AT, O'Brien PCM, Fu B *et al*. Chromosome painting among Proboscidea, Hyracoidea and Sirenia: support for Paenungulata (Afrotheria, Mammalia) but not Tethytheria. *Proceedings of the Royal Society B: Biological Sciences* 2007;**274**:1333–40.
Partha R, Chauhan BK, Ferreira Z *et al*. Subterranean mammals show convergent regression in ocular genes and enhancers, along with adaptation to tunneling. *eLife* 2017;**6**:e25884.
Petter F. Remarques sur la systématique des Chrysochloridés. *Mammalia* 1981;**45**:49–54.
Pickford M. Late Eocene Chrysochloridae (Mammalia) from the Sperrgebiet, Namibia. *Communications of the Geological Survey of Namibia* 2015a;**16**:160–99.
Pickford M. Late Eocene Potamogalidae and Tenrecidae (Mammalia) from the Sperrgebiet, Namibia. *Communications of the Geological Survey of Namibia* 2015b;**16**:121–59.
Pickford M. Tenrecoid mandible from Elisabethfeld (Early Miocene) Namibia. *Communications of the Geological Survey of Namibia* 2018;**18**:87–92.
Pickford M. Tiny Tenrecomorpha (Mammalia) from the Eocene of Black Crow, Namibia. *Communications of the Geological Survey of Namibia* 2019;**21**:15–25.
Pickford M, Senut B, Morales J, *et al*. 2008. Mammalia from the Lutetian of Namibia. *Memoirs of the Geological Survey of Namibia* 2008;**20**:465–514.
Pickford M, Senut B, Mocke H *et al*. Eocene aridity in southwestern Africa: timing of onset and biological consequences. *Transactions of the Royal Society of South Africa* 2014;**69**:139–44.
Pinheiro C, Venter ML, Sahd L *et al*. Comparative gastrointestinal morphology of seven golden mole species (Mammalia: Chrysochloridae) from South Africa. *Journal of Morphology* 2018;**279**:1776–86.
Poux C, Madsen O, Glos J *et al*. Molecular phylogeny and divergence times of Malagasy tenrecs: influence of data partitioning and taxon sampling on dating analyses. *BMC Evolutionary Biology* 2008;**8**:102.
Puttick GM, Jarvis JUM. The functional anatomy of the neck and forelimbs of the Cape golden mole, *Chrysochloris asiatica* (Lipotyphla: Chrysochloridae). *African Zoology* 1977;**12**:445–58.
Puttick MN, Thomas GH. Fossils and living taxa agree on patterns of body mass evolution: a case study with Afrotheria. *Proceedings of the Royal Society B: Biological Sciences* 2015;**282**:20152023.
R Core Team. *R: a Language and Environment for Statistical Computing*. Vienna: R Foundation for Statistical Computing. 2020. https://www.R-project.org/
Rambaut A. *FigTree*. 2018. https://github.com/rambaut/figtree Accessed 26 March 2020.
Rambaut A, Drummond AJ, Xie D *et al*. Posterior summarization in Bayesian phylogenetics using Tracer 1.7. *Systematic Biology* 2018;**67**:901–4.
Reynolds SC, Kibii JM. Sterkfontein at 75: review of paleoenvironments, fauna, dating and archaeology from the hominin site of Sterkfontein (Gauteng Province, South Africa). *Palaeontologia Africana* 2011;**46**:59–88.
Roberts A. *The Mammals of South Africa*. Johannesburg: The Trustees of the Mammals of South Africa Book Fund, 1951.
Ronquist F, Klopfstein S, Vilhelmsen L *et al*. A total-evidence approach to dating with fossils, applied to the early radiation of the Hymenoptera. *Systematic Biology* 2012a;**61**:973–99.
Ronquist F, Teslenko M, Van Der Mark P *et al*. MrBayes 3.2: efficient Bayesian phylogenetic inference and model choice across a large model space. *Systematic Biolology* 2012b;**61**:539–42.
Sallam HM, Seiffert ER. New phiomorph rodents from the latest Eocene of Egypt, and the impact of Bayesian 'clock'-based phylogenetic methods on estimates of basal hystricognath relationships and biochronology. *PeerJ* 2016;**4**:e1717.
Sallam HM, Seiffert ER. Revision of Oligocene '*Paraphiomys*' and an origin for crown Thryonomyoidea (Rodentia: Hystricognathi: Phiomorpha) near the Oligocene–Miocene boundary in Africa. *Zoological Journal of the Linnean Society* 2020;**190**:352–71.
Simonetta AM. A new golden mole from Somalia with an appendix on the taxonomy of the family Chrysochloridae (Mammalia, Insectivora). *Monitore Zoologico Italiano Supplemento* 1968;**2**:27–55.
Skinner JD, Smithers RH. *The Mammals of the Southern African Subregion*. Pretoria: University of Pretoria, 1990.
Smit HA, van Vuuren B, O'Brien PCM *et al*. Phylogenetic relationships of elephant-shrews (Afrotheria, Macroscelididae). *Journal of Zoology* 2011;**284**:133–43.
Stanhope MJ, Waddell VG, Madsen O *et al*. Molecular evidence for multiple origins of Insectivora and for a new order of endemic African insectivore mammals. *Proceedings of the National Academy of Sciences of the United States of America* 1998;**95**:9967–72.
Upham NS, Esselstyn JA, Jetz W. Inferring the mammal tree: species-level sets of phylogenies for questions in ecology, evolution, and conservation. *PLoS Biology* 2019;**17**:e3000494.
Van Couvering JA, Delson E. African land mammal ages. *Journal of Vertebrate Paleontology* 2020;**40**:e1803340.
Vogel P, Odarchenko N, Graf JD. Formule chromosomique de *Micropotamogale lamottei* (Mammalia, Tenrecidae). *Mammalia* 1977;**41**:81–4.
von Mayer A, O'Brien G, Sarmiento EE. Functional and systematic implications of the ear in golden moles (Chrysochloridae). *Journal of Zoology* 1995;**236**:417–30.
Wheeler TJ, Kececioglu JD. Multiple alignment by aligning alignments. *Bioinformatics* 2007;**23**:i559–68.
Wilson DE, Reeder DM. *Mammal Species of the World: a Taxonomic and Geographic Reference*. Baltimore: Johns Hopkins University Press, 2005.